

Varying the Universality of Supersymmetry-Breaking Contributions to MSSM Higgs Boson Masses

John Ellis¹, Keith A. Olive² and Pearl Sandick²

¹TH Division, PH Department, CERN, CH-1211 Geneva 23, Switzerland

²William I. Fine Theoretical Physics Institute,
University of Minnesota, Minneapolis, MN 55455, USA

Abstract

We consider the minimal supersymmetric extension of the Standard Model (MSSM) with varying amounts of non-universality in the soft supersymmetry-breaking contributions to the Higgs scalar masses. In addition to the constrained MSSM (CMSSM) in which these are universal with the soft supersymmetry-breaking contributions to the squark and slepton masses at the input GUT scale, we consider scenarios in which both the Higgs scalar masses are non-universal by the same amount (NUHM1), and scenarios in which they are independently non-universal (NUHM2). We show how the NUHM1 scenarios generalize the $(m_{1=2}; m_0)$ planes of the CMSSM by allowing either m_A or $m_{1=2}$ to take different (fixed) values and we also show how the NUHM1 scenarios are embedded as special cases of the more general NUHM2 scenarios. Generalizing from the CMSSM, we find regions of the NUHM1 parameter space that are excluded because the LSP is a selectron. We also find new regions where the neutralino relic density falls within the range preferred by astrophysical and cosmological measurements, thanks to rapid annihilation through direct-channel Higgs poles, or coannihilation with selectrons, or because the LSP composition crosses over from being mainly bino to mainly Higgsino. Generalizing further to the NUHM2, we find regions of its parameter space where a sneutrino is the LSP, and others where neutralino coannihilation with sneutrinos is important for the relic density. In both the NUHM1 and the NUHM2, there are slivers of parameter space where the LHC has fewer prospects for discovering particles than in the CMSSM, because either $m_{1=2}$ and/or m_0 may be considerably larger than in the CMSSM.

1 Introduction

The simplest supersymmetric model is the minimal supersymmetric extension of the Standard Model (MSSM), and it is commonly assumed that the soft supersymmetry-breaking contributions to the squark, slepton and Higgs scalar masses are universal at some GUT input scale (CMSSM) [1,2]. This is certainly the simplest assumption, but it is neither the only nor necessarily the most plausible version of the MSSM. For example, universality might hold at some lower renormalization scale [3], as in some mirage unification scenarios [4]. Alternatively, the soft supersymmetry-breaking masses may not be universal at any renormalization scale, as occurs in some string scenarios for supersymmetry breaking [5]. The suppression of flavour-changing supersymmetric interactions suggests that the soft supersymmetry-breaking masses of all generations of squarks and sleptons with the same electroweak quantum numbers may be the same, i.e., $m_{\tilde{e}_L}^2 = m_{\tilde{\nu}_L}^2 = m_{\tilde{\tau}_L}^2$, $m_{\tilde{e}_R}^2 = m_{\tilde{\nu}_R}^2 = m_{\tilde{\tau}_R}^2$, and similarly for the $q_{L,R}$ of charges $+2/3$ and $-1/3$ [6]. However, this argument does not motivate universality between sleptons and squarks, or even between left- and right-handed sleptons or squarks. Some degree of universality would be expected in supersymmetric GUTs. For example, in supersymmetric SU(5) one would expect $m_{\tilde{e}_L}^2 = m_{\tilde{d}_R}^2$ and $m_{\tilde{e}_R}^2 = m_{\tilde{u}_L}^2 = m_{\tilde{u}_R}^2$. Supersymmetric SO(10) would further predict universality between all the soft supersymmetry-breaking squark and slepton masses. However, supersymmetric GUTs do not give any reason to think that the soft supersymmetry-breaking contributions to the Higgs scalar masses should be universal with the squark and slepton masses. This full universality, postulated in the CMSSM, would occur in minimal supergravity (mSUGRA) scenarios [7], but not in more general effective no-scale supergravity theories such as those derived from string models [8].

On the basis of the above discussion, it is natural to consider models with non-universal soft supersymmetry-breaking contributions to the Higgs scalar masses [9]. In general, one may introduce two independent non-universality parameters, scenarios which can be termed NUHM2 [10], but one could also consider scenarios with equal amounts of non-universality for the two Higgs doublets, scenarios which can be termed NUHM1 [11]. Such scenarios would be natural in a supersymmetric SO(10) GUT framework, since the two Higgs multiplets occupy a common vectorial 10-dimensional representation, while each matter generation occupies a common spinorial 16-dimensional representation of SO(10).

CMSSM scenarios have four continuous parameters, which may be taken as m_0 ; $m_{1=2}$; A_0 ; $\tan\beta$, with the values of j and m_A then being fixed by the electroweak vacuum conditions. Correspondingly, NUHM1 scenarios have one additional parameter, that may be taken as either μ or m_A , whereas both μ and m_A are free parameters in NUHM2 scenarios. The full six-dimensional NUHM2 parameter space has been explored in a number of studies [10], but its higher dimensionality renders its complete characterization quite complicated, and it is less amenable to a Markov Chain Monte Carlo analysis than the NUHM1 and particularly CMSSM scenarios [12]. The main purpose of this paper is to discuss how the CMSSM, NUHM1 and NUHM2 scenarios may be related by processes of dimensional enhancement: CMSSM \rightarrow NUHM1 \rightarrow NUHM2 and reduction: NUHM2 \rightarrow NUHM1 \rightarrow CMSSM, laying the basis for more complete understanding of the NUHM1 and NUHM2 parameter spaces. Accordingly, in the following sections we focus first on the relationship between the CMSSM and

NUHM 1 scenarios, and subsequently on the relationship between the NUHM 1 and NUHM 2 scenarios.

The most important contributions to most sparticle masses are those due to $m_{1=2}$ and m_0 , so studies of the phenomenological constraints on the CMSSM parameter space [13,14] and the prospects for experimental searches at the LHC and elsewhere are frequently displayed in $(m_{1=2}; m_0)$ planes for different values of $\tan\beta$, A_0 and the sign of μ . The values of j and m_A then vary across these planes according to the electroweak vacuum conditions. In our first exploration of the NUHM 1 parameter space, we display and discuss $(m_{1=2}; m_0)$ planes for different choices of fixed values of m_A and positive μ , seeking to understand, in particular, the dependences on m_A and μ of the strips of parameter space compatible with the cold dark matter density inferred from WMAP and other observations [15]. A key question here is whether the good (but not complete) LHC coverage of the CMSSM WMAP strips [13] is repeated also in NUHM 1 scenarios. We find that there are extensions of the preferred regions of the $(m_{1=2}; m_0)$ planes to larger values of these parameters that are affected by the choices of μ or m_A , whereas the preferred regions of these latter parameters are more sensitive to the choices of the other NUHM 1 parameters. In some of the extensions, the LHC would either have difficulty in detecting supersymmetry at all, or would only provide access to a limited range of sparticles. Since the interest of NUHM 1 scenarios lies largely with the new possibilities for varying m_A and μ , which have in turn important implications for the spectrum of heavy MSSM Higgs bosons and gauginos, we also display explicitly the variations of the various phenomenological constraints in planes correlating $m_{1=2}$ or m_0 with m_A or μ .

In our discussion of the relationship between the NUHM 1 and NUHM 2 scenarios, we display the allowed regions of parameter space as explicit functions of the degrees of non-universality of the soft supersymmetry-breaking scalar mass parameters of the two MSSM Higgs multiplets. We find that the WMAP relic density constraint, in particular, generally favours models with a relatively high degree of non-universality, close to the boundaries of the NUHM 2 parameter space imposed by other theoretical and phenomenological constraints such as the breakdown of electroweak symmetry breaking or the absence of charged dark matter. This reflects the fact, known already from studies of the CMSSM with GUT-scale universality, that the supersymmetric relic density is too large in generic domains of parameter space, being brought down into the WMAP range in particular cases such as the coannihilation [16] and focus-point regions (close to the charged dark matter and electroweak symmetry breaking boundaries, respectively) [17], or in rapid-annihilation funnel regions [1].

2 From the CMSSM to the NUHM 1

In the CMSSM, the weak-scale observables are determined by four continuous parameters and a sign; the universal scalar mass m_0 , the universal gaugino mass $m_{1=2}$, the universal trilinear coupling A_0 , the ratio of the Higgs vacuum expectation values $\tan\beta$, and the sign of the Higgs mass parameter μ . We consider the values of the parameters m_0 , $m_{1=2}$ and A_0 to be specified at the SUSY GUT scale. The effective Higgs masses squared, m_1^2 and m_2^2 are responsible for generating electroweak symmetry breaking through their running from the

input scale down to low energies. In the CMSSM, $m_1^2(M_{\text{GUT}}) = m_2^2(M_{\text{GUT}}) = m_0^2$, and $\tan\beta$ and m_A are calculated from the electroweak vacuum conditions,

$$m_A^2(Q) = m_1^2(Q) + m_2^2(Q) + 2\mu^2(Q) + \delta_A^{(1)}(Q) \quad (1)$$

and

$$\tan\beta = \frac{m_1^2 - m_2^2 \tan^2\beta + \frac{1}{2}m_Z^2(1 - \tan^2\beta) + \delta^{(1)}}{\tan^2\beta - 1 + \delta^{(2)}}; \quad (2)$$

where $\delta_A^{(1)}$ and $\delta^{(2)}$ are loop corrections [18,20], $Q = (m_{\tilde{\tau}_R} m_{\tilde{\tau}_L})^{1=2}$, and all quantities in (2) are defined at the electroweak scale, m_Z . Unless otherwise noted, $m_A = m_A(Q)$ and $\mu = \mu(m_Z)$. The values of the parameters in (1) and (2) are related through well-known radiative corrections [18,21,22] c_1, c_2 and c such that

$$\begin{aligned} m_1^2(Q) &= m_1^2 + c_1; \\ m_2^2(Q) &= m_2^2 + c_2; \\ \mu^2(Q) &= \mu^2 + c; \end{aligned} \quad (3)$$

In the NUHM1 one still has $m_1^2(M_{\text{GUT}}) = m_2^2(M_{\text{GUT}})$, but these are no longer identified with the universal scalar mass, m_0 , so an additional parameter is necessary to fix the common GUT-scale value of the Higgs masses-squared. This additional parameter may be taken to be either μ or m_A , and the relationship between m_1^2 and m_2^2 at the weak scale can be calculated from (1) – (3) so as to respect the electroweak boundary conditions at m_Z and the weakened universality condition at M_{GUT} .

If m_A is taken to be the free parameter (input), then at m_Z we have

$$\begin{aligned} m_1^2(\tan^2\beta + 1 + \delta^{(2)}) &= m_2^2(\tan^2\beta + 1 - \delta^{(2)}) + m_Z^2(\tan^2\beta - 1) - 2\mu^2 \\ &+ m_A^2(\delta_A^{(1)}(Q) + c_1 + c_2 + 2c)(\tan^2\beta - 1 + \delta^{(2)}); \end{aligned} \quad (4)$$

Alternatively, if μ is taken as the free parameter, then at m_Z we have

$$m_1^2 = m_2^2 \tan^2\beta + \mu^2(\tan^2\beta - 1 + \delta^{(2)}) + \frac{1}{2}m_Z^2(\tan^2\beta - 1) - \mu^2; \quad (5)$$

In each case, the boundary condition at M_{GUT} is $m_1^2 = m_2^2$. Clearly, for some specific input values of μ and m_A , one finds $m_1^2(M_{\text{GUT}}) = m_2^2(M_{\text{GUT}}) = m_0^2$, thereby recovering the CMSSM. The characteristics of the parameter space as one deviates from this scenario are the subjects of the following subsections.

2.1 The NUHM1 with m_A as a Free Parameter

We begin our characterization of the relationship between the CMSSM and NUHM1 scenarios by taking m_A as the additional free parameter, and assume positive μ , as suggested by $g_{\tau\tau}^2$ and $b\tau s$, at least within the CMSSM.

As a basis for the comparison, in Fig. 1 we show in panel (a) a CMSSM ($m_{1=2}, m_0$) plane with $\tan\beta = 10$ and $A_0 = 0$. We have plotted (pink) contours of constant μ and m_A of

300, 500, 1000, and 1500 GeV, with contours appearing roughly vertical and m_A contours appearing as quarter-ellipses centered at the origin. There are also several phenomenological constraints shown in panel (a)¹. In the region at low $m_{1=2}$ and large m_0 there is a (dark pink) shaded region where there are no consistent solutions to the electroweak vacuum conditions, since they would require $\mu^2 < 0$. An additional unphysical region is found along the bottom of the plane at larger $m_{1=2}$ and low m_0 , where the lightest supersymmetric particle (LSP) is a charged stau $\tilde{\tau}$ (brown shading). Contours of $m_h = 114$ GeV (red dot-dashed) and $m_h = 104$ GeV (black dashed) mark, approximately, the edges of the regions excluded by unsuccessful searches at LEP [23]. Both m_h and $m_{1=2}$ increase with $m_{1=2}$, so portions to the right of these contours are allowed. The region favored by the measurement of the muon anomalous magnetic moment [24], $g - 2$, at the two-level (light pink shading bounded by solid black lines) is also visible at very low ($m_{1=2}; m_0$), and the region disfavoured by $b \rightarrow s \gamma$ [25] is shaded green.

Finally, the regions of the plane where the relic density of neutralino LSPs falls in the range favoured by WMAP and other observations for the dark matter abundance appear as thin turquoise strips. For the chosen value of $\tan \beta = 10$, the relic density of neutralinos is too large over the bulk of the plane, and falls within the WMAP range in two distinct regions. In the upper left corner, tracking the region excluded by the electroweak vacuum conditions, lies the focus-point region [17], where the lightest neutralino is Higgsino-like and annihilations to gauge bosons bring the relic density down into the WMAP range. Alongside the forbidden $\tilde{\tau}$ -LSP region lies the coannihilation strip [16], where $\tilde{\tau}$ -coannihilations reduce the relic density of neutralinos. At larger $\tan \beta$, a rapid-annihilation funnel [1] may exist where $2m_{\tilde{\tau}} \approx m_A$ and s -channel annihilations mediated by the pseudoscalar Higgs decrease drastically the relic density of neutralino LSPs, though not for $\tan \beta = 10$. We see that the CMSSM predicts values of m_A between 500 GeV and 1500 GeV and between 500 GeV and 1200 GeV in the parts of the coannihilation strips compatible with the LEP constraints, while values of $m_A > 1500$ GeV and $m_A < 500$ GeV are favoured in the focus-point region for $m_0 < 2$ TeV.

Panels (b), (c), and (d) of Fig. 1 show NUHM1 ($m_{1=2}; m_0$) planes for $\tan \beta = 10; A_0 = 0$ and $\mu > 0$ with $m_A = 500, 1000, \text{ and } 1500$ GeV, respectively, and $\Omega_{\tilde{\chi}_0^0}$ calculated using (2). In addition to the constraints discussed above, we also plot contours of $\Omega_{\tilde{\chi}_0^0} = 300, 500, 1000, \text{ and } 1500$ GeV (light pink). The most prominent departure from the CMSSM is that the requirement of electroweak symmetry breaking constrains the plane at low m_0 rather than at large m_0 . In this region (below the CMSSM contour), m_A is fixed to be larger than its CMSSM value, resulting in correspondingly larger m_1^2 and m_2^2 . We see from (2) that, with $m_2^2 < 0$ and weighted by $\tan^2 \beta$, the effect is to drive μ^2 smaller, and eventually negative. The excluded region grows with m_A as m_1^2 and m_2^2 are pushed farther from their CMSSM values, and isanked by concentric contours of constant $\Omega_{\tilde{\chi}_0^0}$. The stau LSP exclusion regions are qualitatively similar to those in the CMSSM, shown in panel (a), however for moderate values of m_A there is a (black shaded) region of the plane where the lighter selectron is the LSP. Also apparent in panel (b) for $m_0 = 300$ GeV is a small region at low $m_{1=2}$ and m_0 that is favored by $g - 2$, which disappears for larger m_A beneath the expanding region where

¹We use the same notations for these constraints in this and the following figures.

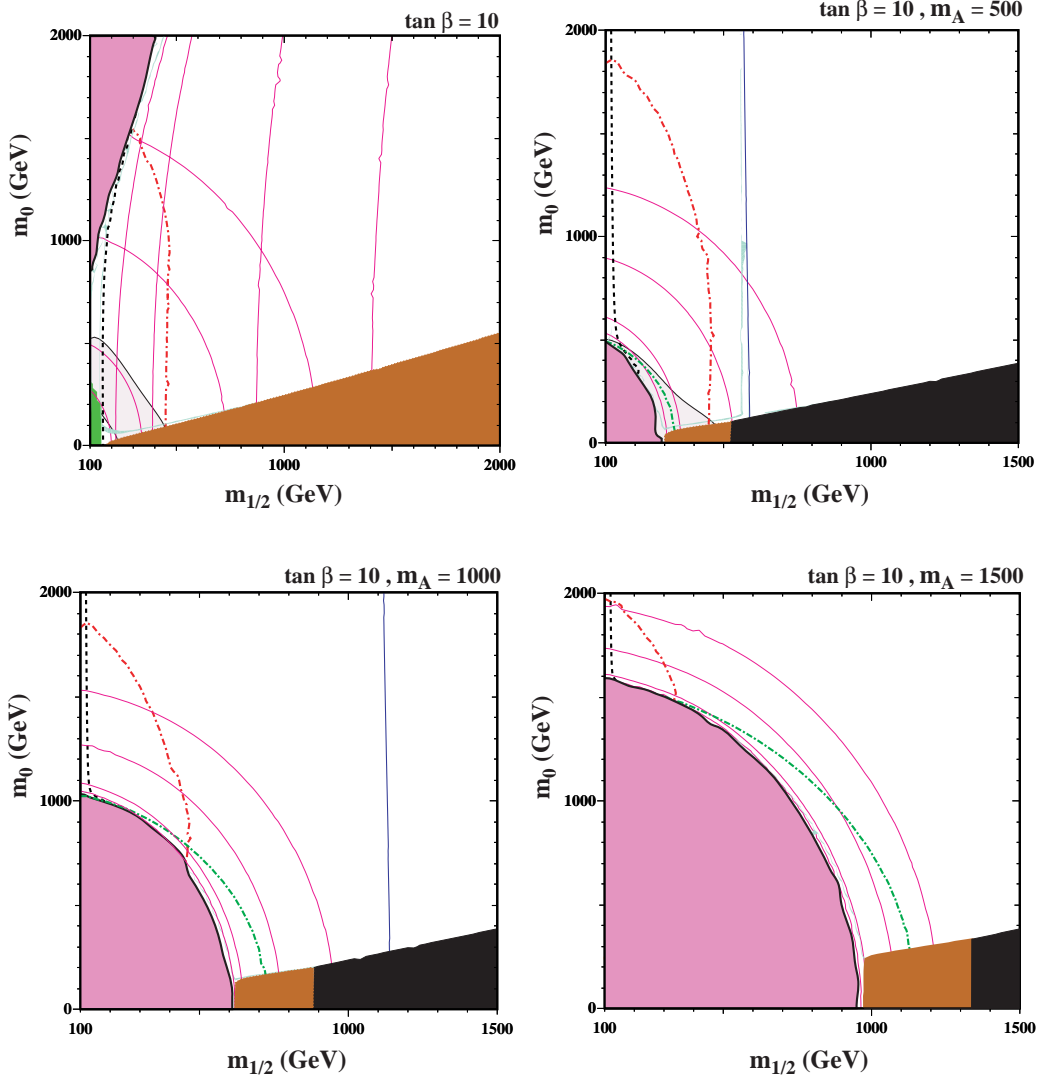


Figure 1: Panel (a) shows the $(m_{1=2}; m_0)$ plane for the CMSSM for $\tan \beta = 10$, with contours of m_A and μ of 300, 500, 1000, and 1500 GeV as described in the text. Panels (b), (c), and (d) show the NUHM1 $(m_{1=2}; m_0)$ planes for $\tan \beta = 10$ with $m_A = 500, 1000$, and 1500 GeV, respectively. Constraints and contours are as described in the text.

electroweak symmetry breaking is not possible. There is no region of this or the following panels that is excluded by $b \rightarrow s \gamma$.

The LSP mass and composition are roughly the same as they are in the CMSSM at large μ : at all but the smallest values of μ , the LSP is bino-like in the CMSSM. At moderate and large μ , the masses of the sparticles are only minimally affected by the fact that m_A is fixed, causing several of the constraints to appear similar to the CMSSM case. In particular, the LEP chargino and Higgs constraints again exclude smaller values of $m_{1=2}$, though the shape

of both the Higgs and the chargino exclusions change with increasing m_A .

The strip where the relic LSP density falls within the range preferred by WMAP and other data stays, in general, close to the regions excluded by the requirement that the LSP be neutral and by the electroweak vacuum conditions. However, one difference from the CMSSM for $\tan\beta = 10$ that is very prominent in panel (b) is a rapid-annihilation funnel, straddling the dark blue contour where $2m_{\tilde{1},2} = m_A$, that rises out of the coannihilation strip at $m_{1=2} = 570$ GeV, reaching $m_0 \approx 2300$ GeV. Branches of good relic density form the inner and outer funnel walls, between which the relic density falls below the WMAP range. At larger m_A , the dark matter strip changes somewhat. For $m_A = 1000$ GeV, shown in panel (c) of Fig. 1, $2m_{\tilde{1},2} = m_A$ at $m_{1=2} = 1130$ GeV. However the coannihilation strip has essentially terminated at lower $m_{1=2}$, so there is no prominent rapid-annihilation funnel. Finally, at $m_A = 1500$ GeV, shown in panel (d), $2m_{\tilde{1},2} = m_A$ at $m_{1=2} = 1680$ GeV, well beyond the end of the coannihilation strip. The relic density still decreases in these regions, but it remains above the WMAP range, so there is no visible funnel.

We have already emphasized that the parameter space expands by one dimension between the CMSSM and the NUHM1. In each plane (b)–(d) of Fig. 1, there is a green dot-dashed contour tracking the CMSSM parameters in the NUHM1 ($m_{1=2}; m_0$) plane. The change in position of this contour as m_A is increased can be understood by comparison with the contours of constant m_A in the CMSSM panel (a). As an example, we consider the variation in μ on the CMSSM contour and how its position changes in the NUHM1 plane. Examining the contour of $m_A = 1000$ GeV in the CMSSM plane, we find that in the \sim -LSP region, the value of μ along the contour reaches a maximum of about 860 GeV. Following the curve to larger m_0 , we see that it terminates at the boundary of the region where $\mu^2 < 0$. So we expect that the CMSSM contour in the NUHM1 ($m_{1=2}; m_0$) plane with $m_A = 1000$ GeV runs smoothly through the contours of constant μ from $\mu = 860$ GeV in the \sim -LSP region to the boundary of the electroweak symmetry breaking region. As m_A increases, the CMSSM contour begins near the coannihilation strip at correspondingly larger values of μ , but it always terminates at $\mu = 0$. The points of intersection of the CMSSM line with the electroweak vacuum boundary move to larger values of $m_{1=2}$ and m_0 as m_A increases in panels (b), (c) and (d), tracking the focus-point region in panel (a).

It is clear from panels (b) to (d) that the NUHM1 shares some small pieces of the cosmologically preferred regions of the parameter space of the CMSSM for moderate and large values of m_A . Only for 500 GeV $< m_A < 1500$ GeV does the CMSSM contour intersect a phenomenologically viable portion of the coannihilation strip, and only for $m_A \approx 1500$ GeV does it intersect the focus-point region. Moving away from the CMSSM contours in the NUHM1 planes, we find that cosmologically preferred areas in the focus-point regions are now available at lower m_A . For example, at $m_A = 1000$ GeV in the CMSSM, the focus-point is found at low values of $m_{1=2}$ where both the Higgs and chargino mass constraints are violated. In the NUHM1, as seen in panel (c), we find a viable focus-point strip at $m_{1=2} > 500$ GeV at values of μ lower than in the CMSSM. Furthermore, we find additional coannihilation strip at both larger and smaller μ than what would be expected in the CMSSM, and for a range of m_A there is even a rapid-annihilation funnel.

The funnel region is interesting in that it passes all constraints and may have fairly heavy

scalars, as does the focus-point region in the CM SSM, but with a bino-like neutralino LSP. A key difference between the two cases is illustrated by the following simple example. If the LHC discovers a gluino weighing 1.5 TeV, which is estimated to be possible with less than 1 fb^{-1} of integrated luminosity [26–28], then, in the CM SSM the lightest charged sparticles are encouragingly light with $m_{\tilde{c}} = 340 \text{ GeV}$ in the focus-point region and $m_{\tilde{c}} = 280 \text{ GeV}$ in the coannihilation strip. However, in the NUHM1, although we will discover charged staus easily if Nature has chosen the coannihilation strip, at the peak of the funnel in panel (b) the lighter chargino could be heavier than 900 GeV, and staus would be as heavy as $m_{\tilde{\tau}} = 2300 \text{ GeV}$. In this case, the rapid-annihilation funnel represents a continuum of viable sparticle masses between the two extremes. Both the CM SSM points and the NUHM1 points have a light LSP with $250 \text{ GeV} < m_{\tilde{\chi}_1^0} < 280 \text{ GeV}$, but the pseudoscalar Higgs mass is quite large in the CM SSM and highly dependent on the value of m_0 , whereas in the NUHM1 $m_A = 550 \text{ GeV}$ in this case. According to previous studies in the CM SSM, detecting supersymmetry at the LHC should be possible along the rapid-annihilation strip in panel (b) for $m_0 < 2000 \text{ GeV}$ with roughly 10 fb^{-1} of integrated luminosity, though the number of sparticles accessible with dedicated follow-up searches would decrease as m_0 increases.

2.1.1 Fixed m_0

Alternative ways to view the NUHM1 parameter space include fixing either m_0 or $m_{1=2}$ and scanning over m_A . We first examine the former option.

We show in Fig. 2 examples of the $(m_A; m_{1=2})$ planes for $m_0 = 300, 500, 1000$, and 1500 GeV . The unfamiliar appearances of the constraints can once again be understood by comparison with panel (a) of Fig. 1. For example, for $m_0 = 300 \text{ GeV}$, as seen in panel (a), we note that the upper third of the plane is excluded due to a charged LSP. This reflects the fact that in the CM SSM plane, for fixed m_0 , $m_{\tilde{\chi}_1^0}$ increases more slowly than $m_{\tilde{c}}$ as $m_{1=2}$ increases, so that at large $m_{1=2}$ the $\tilde{\chi}_1^0$ becomes the LSP. Increasing m_0 postpones the $\tilde{\chi}_1^0$ -LSP region to larger $m_{1=2}$, so that this constraint almost disappears in panel (b) where $m_0 = 500 \text{ GeV}$, and does not appear at all in panels (c) and (d), where $m_0 = 1000$ and 1500 GeV , respectively. While there is no \tilde{e} -LSP region in the CM SSM plane, as seen in panel (a) of Fig. 1, the selectron mass renormalization is similar to that of the stau, so the selectron-LSP regions in the NUHM1 planes shift similarly to larger $m_{1=2}$.

The other unphysical regions in CM SSM planes occur in their upper left corners, where there is no consistent electroweak vacuum. As seen in panel (a) of Fig. 1, this issue arises at low $m_{1=2}$ and large m_0 . As m_0 is increased, the boundary of this region moves to larger $m_{1=2}$ and m_A . The positive correlation between m_A and $m_{1=2}$ along this boundary is seen clearly in all the panels of Fig. 2. We also see that, particularly at small $m_{1=2}$, this boundary also retreats to larger m_A as m_0 increases. Following the boundary of this excluded region are the contours of constant β , which converge slightly as m_A and $m_{1=2}$ increase. Also apparent in panel (a) for $m_0 = 300 \text{ GeV}$ is a small region at low $m_{1=2}$ and m_0 that is favored by $g_{\tilde{c}} > 2$, which disappears for larger m_0 . We also see at very low $m_{1=2}$ the LEP chargino bound. The dominant experimental constraints in these planes are the LEP limits on the Higgs mass and the branching ratio of $b \rightarrow s \gamma$, which exclude the areas below the dot-dashed red contour

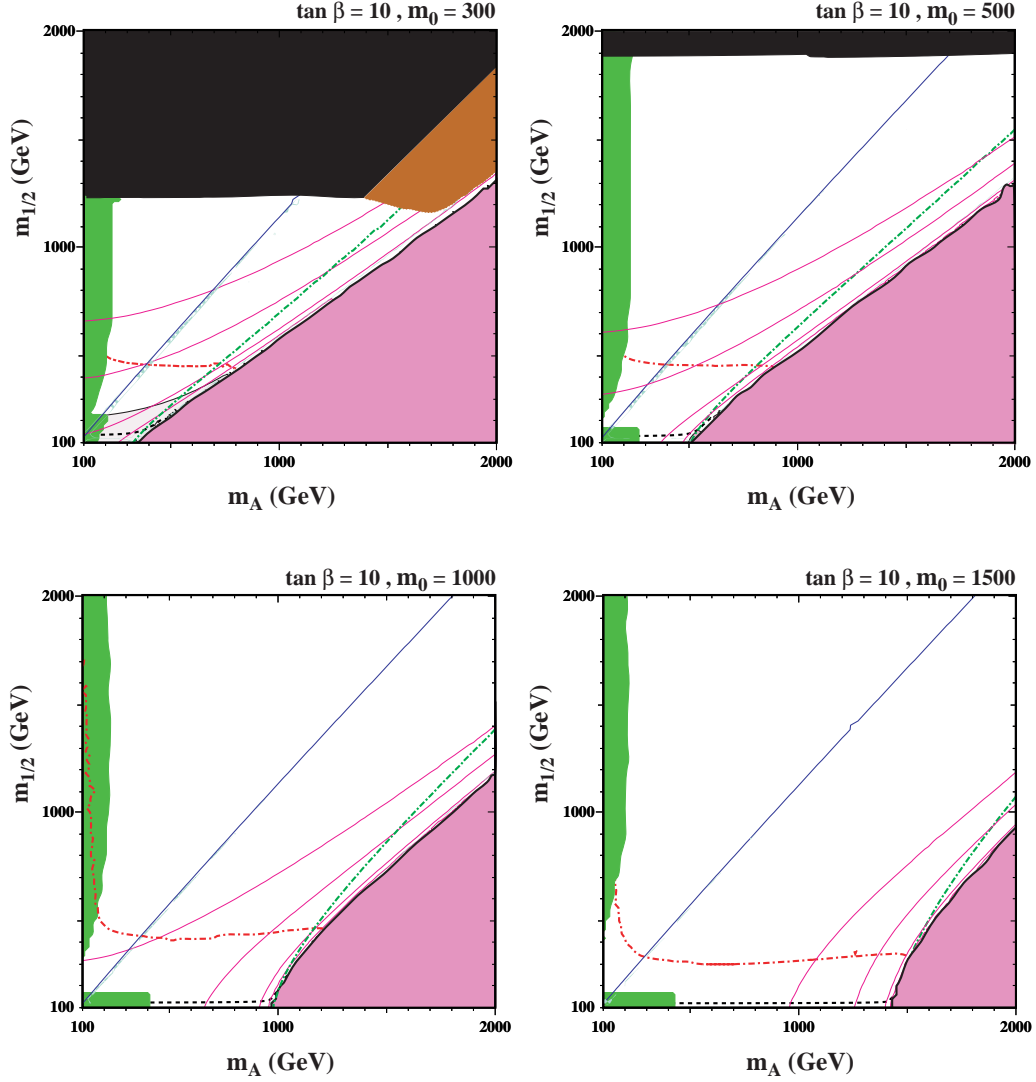


Figure 2: Examples of NUHM1 (m_A ; $m_{1=2}$) planes with $\tan \beta = 10$, $A_0 = 0$, $\mu > 0$, and $m_0 = 300, 500, 1000,$ and 1500 GeV in Panels (a), (b), (c), and (d), respectively. Constraints are displayed as in Figure 1.

and in the green shaded region, respectively.

There are two viable WMAP-compatible regions in these planes. One is the upper portion of the rapid-annihilation funnel, which is oriented diagonally in the planes, close to the diagonal blue line where $m_{1=2} = m_A = 2$. Since the position of the funnel is defined by the LSP mass, which in this case depends primarily on $m_{1=2}$ due to its bino-like character, and the pseudoscalar Higgs mass, which forms the x-axis, the rapid-annihilation funnel is fixed in the plane as m_0 is varied. The other viable WMAP-compatible region (less immediately apparent in these plots) is the focus-point region which tracks the boundary of the region

where electroweak symmetry breaking is not possible.

In each plane of Fig. 2, the CMSSM contour runs diagonally through the contours of constant Ω . For $m_0 = 300$ GeV, the CMSSM contour starts in the bulk region at low $m_{1=2}$. Many of these points lie in the region favored by $g < 2$, but this portion of the plane is excluded by the LEP bound on the Higgs mass. As we follow the CMSSM contour to larger $m_{1=2}$ (larger m_A), we see that Ω is increasing along the contour. This corresponds to following a contour of constant m_0 horizontally across the CMSSM ($m_{1=2}; m_0$) plane. Eventually, at large $m_{1=2}$ and any fixed value of m_0 , the CMSSM contour intersects the region where the $\tilde{\nu}$ is the LSP, but not the \tilde{e} -LSP region. As we increase m_0 , the $\tilde{\nu}$ -LSP region is postponed to larger $m_{1=2}$. The CMSSM contours at large m_0 lie above the bulk region, but the LEP constraint on the Higgs mass is still important, as it is only very weakly dependent on m_0 . The rapid-annihilation funnel region of WMAP-compatible neutralino relic density is bounded at low $m_{1=2}$ by the LEP Higgs constraint and, for low m_0 , at large $m_{1=2}$ by the $\tilde{\nu}$ -LSP region. The funnel occurs at larger Ω than we expect in the CMSSM.

According to previous studies [26,27], the LHC should find a signal of supersymmetry in the CMSSM scenario with 10 fb^{-1} of integrated luminosity if $m_{1=2} = 900(900)(800)(700)$ GeV for $m_0 = 300(500)(1000)(1500)$ GeV. In the NUHM1, for fixed $m_{1=2}$ and m_0 , the spectrum of charged scalars and gauginos is only affected through loop corrections to the RGEs, so we expect a similar LHC reach for these values of m_0 , shown in panels (a, b, c) and (d) of Fig. 2. This means that progressively shorter sections of the rapid-annihilation funnels and focus-point strips are likely to be accessible to the LHC.

2.1.2 Fixed $m_{1=2}$

We now discuss NUHM1 parameter space for various fixed values of $m_{1=2}$, as shown in the ($m_A; m_0$) planes in Fig. 3. We note first that the forbidden stau LSP region is absent for low $m_{1=2} = 300$ GeV, as seen in panel (a), puts in an appearance at low m_0 when $m_{1=2} = 500$ GeV, as seen in panel (b), and reaches progressively to larger m_0 at larger $m_{1=2}$, as seen in panels (c) and (d). This behaviour was to be expected from the analogous feature in the CMSSM, shown in panel (a) of Fig. 1, and reflects the fact that $m_{\tilde{\nu}}$ increases more rapidly with $m_{1=2}$ than does $m_{\tilde{\tau}}$. At larger $m_{1=2}$ we see the emergence of the selectron LSP region at low m_A . We also note that the electroweak vacuum exclusion retreats to smaller m_0 and larger m_A as $m_{1=2}$ increases, disappearing altogether for $m_{1=2} = 1000$ and 1500 GeV, again reflecting the CMSSM feature seen in panel (a) of Fig. 1.

One of the dominant experimental constraints on the parameter space is that due to the LEP Higgs mass bound, which excludes most of the plane for $m_{1=2} = 300$ GeV and low m_A for $m_{1=2} = 500$ GeV, as seen in panels (a) and (b), respectively. The Higgs mass is more sensitive to variations in m_0 at lower $m_{1=2}$, whereas at large $m_{1=2}$ the Higgs mass is primarily sensitive to $m_{1=2}$ and less dependent on m_0 (as in the CMSSM). We also note that the branching ratio of $b \rightarrow s\gamma$ excludes a strip of parameter space that expands slowly with m_A .

There are three distinct regions of WMAP-compatible relic density in these ($m_A; m_0$) planes. The first is the vertical rapid-annihilation funnel, where the relic density decreases

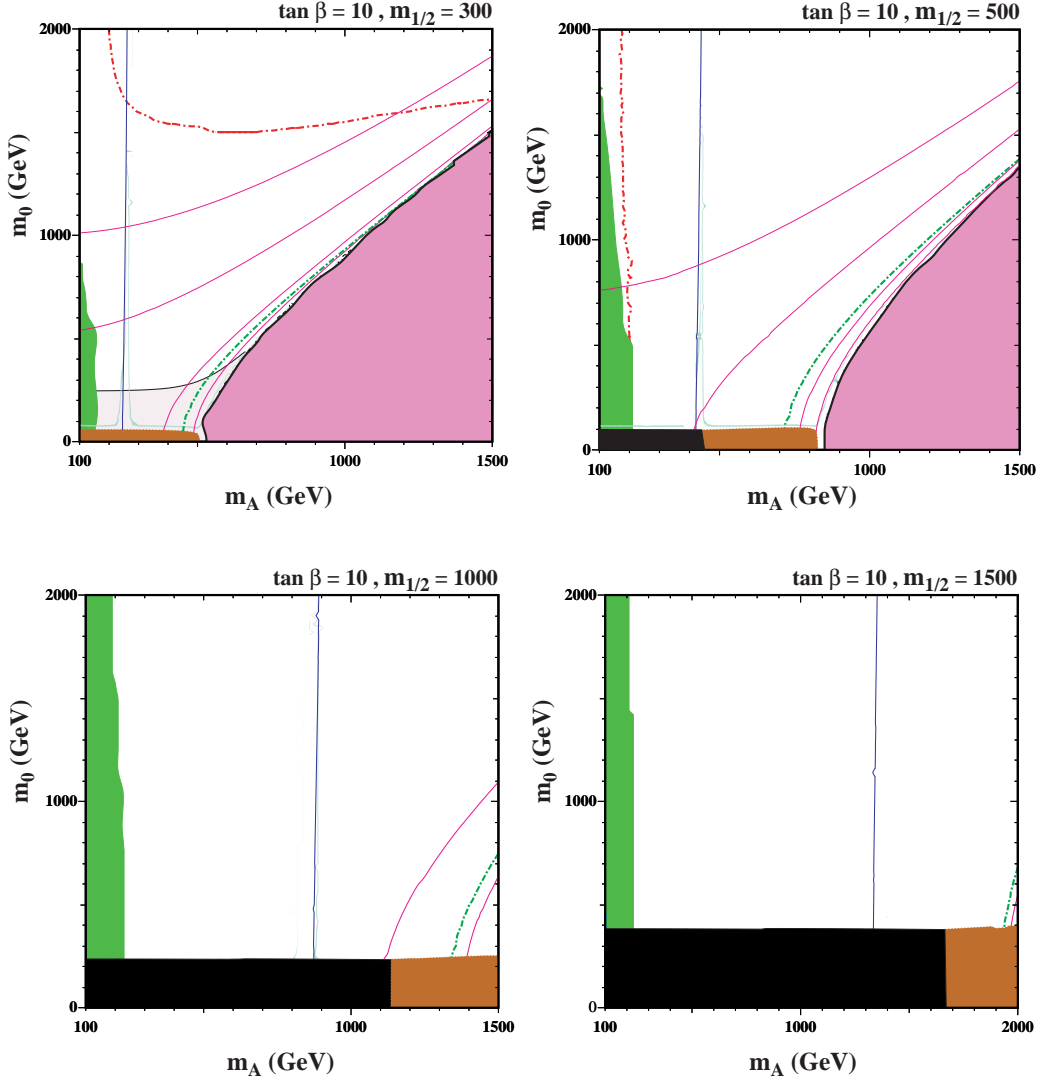


Figure 3: Examples of NUHM 1 $(m_A; m_0)$ planes with $\tan \beta = 10$, $A_0 = 0$, $\mu > 0$, and $m_{1/2} = 300, 500, 1000$, and 1500 GeV in Panels (a), (b), (c), and (d), respectively. Constraints are displayed as in Figure 1.

drastically. This moves to larger m_A as $m_{1/2}$ increases, reflecting the movement of the blue line where $m_{1/2} = m_A = 2$. The second region of good relic density is the coannihilation strip, which is present when $m_{1/2} > 900$ GeV. In fact, we see that the rapid-annihilation funnel rises directly out of the coannihilation strip where the two coincide, as also seen in Fig. 1. Finally, the third is the focus-point strip, which tracks the region excluded by the requirement of electroweak symmetry breaking. As $m_{1/2}$ continues to increase, this strip is pushed to values of m_A beyond those plotted.

The CMSSM contours in the $(m_A; m_0)$ planes correspond to following a strip of constant

$m_{1=2}$ in the $(m_{1=2}; m_0)$ plane shown in panel (a) of Fig. 1 upwards from the coannihilation strip. Since μ depends strongly on $m_{1=2}$, but has little sensitivity to the value of m_0 , these contours appear to be roughly contours of constant μ in each case. For low values of $m_{1=2}$, the CM SSM contour begins in the bulk region at low m_0 . This is a region favoured by $g_{\text{eff}} = 2$ but strongly excluded by the LEP Higgs bound. Eventually, we find the focus-point region at very large m_0 . In panel (b), the CM SSM line arches up from the \sim -LSP region towards the region where there is no electroweak symmetry breaking. In Panels (c) and (d), the CM SSM contour begins at low m_0 and large m_A in the \sim -LSP region, but there are no further visible features of interest. As already noted, both the CM SSM contour and the rapid annihilation funnel move to larger m_A as $m_{1=2}$ increases. However, since the CM SSM contour moves more quickly than the funnel, there is no rapid annihilation funnel in the CM SSM for $\tan\beta = 10$, unlike the NUHM 1 case.

According to previous studies [26,27], the LHC should find a signal of supersymmetry in the CM SSM scenario with 10 fb^{-1} of integrated luminosity if $m_0 < 2000 \text{ GeV}$ for $m_{1=2} = 300(500) \text{ GeV}$. As discussed in section 2.1.1, we expect a similar reach in the NUHM 1 for comparable values of $m_{1=2}$, as shown in panels (a) and (b) of Fig. 1. This means that all of the visible parts of these planes should be accessible to the LHC. On the other hand, previous analyses [26,27] suggest that in the CM SSM, the parameter space with $m_{1=2} \lesssim 1000 \text{ GeV}$ would be inaccessible without an increase in the integrated luminosity. In the NUHM 1 planes, due to the appearance of the rapid-annihilation funnel, one may find fairly light charged scalars even if $m_{1=2} > 1000 \text{ GeV}$, as shown in panels (c) and (d).

2.1.3 Varying $\tan\beta$

Finally, we discuss the characteristics of the NUHM 1 parameter space as we vary $\tan\beta$. We recall that in the CM SSM at large $\tan\beta$ a rapid-annihilation funnel appears in the $(m_{1=2}; m_0)$ plane when $\tan\beta > 35$, extending from the coannihilation strip to larger $(m_{1=2}; m_0)$. In addition, at large $\tan\beta$ the excluded \sim -LSP region becomes more prominent in the $(m_{1=2}; m_0)$ plane at low m_0 , and the branching ratio of $b \rightarrow s \gamma$ excludes more of the plane at low $m_{1=2}$ ². The effects of variations in $\tan\beta$ on these constraints alter the appearance of the NUHM 1 planes, as well.

In Fig. 4, we show NUHM 1 $(m_A; m_{1=2})$ planes with $m_0 = 500 \text{ GeV}$ and $\tan\beta = 10, 20, 35$, and 50 in panels (a), (b), (c), and (d), respectively. Note that panel (a) of Fig. 4 is the same as panel (b) of Fig. 2. As $\tan\beta$ is increased, μ decreases, as is evidenced by the movement of the contours of constant μ out into the plane and the expansion of the region where there are no consistent solutions to the electroweak vacuum conditions. As a result, the CM SSM contour is pushed to lower m_A for fixed $m_{1=2}$, moving closer to the rapid-annihilation funnel. In the CM SSM, however, the rapid-annihilation funnel begins at roughly $m_0 = 800 \text{ GeV}$, so the CM SSM contour does not cross the rapid-annihilation funnel even at $\tan\beta = 50$ in these planes with $m_0 = 500 \text{ GeV}$. In these NUHM 1 planes, the location of the rapid-annihilation funnel is almost independent of $\tan\beta$.

²Moderate cancellations between different contributions, that sometimes introduce an allowed corridor through the excluded region, even at low $m_{1=2}$.

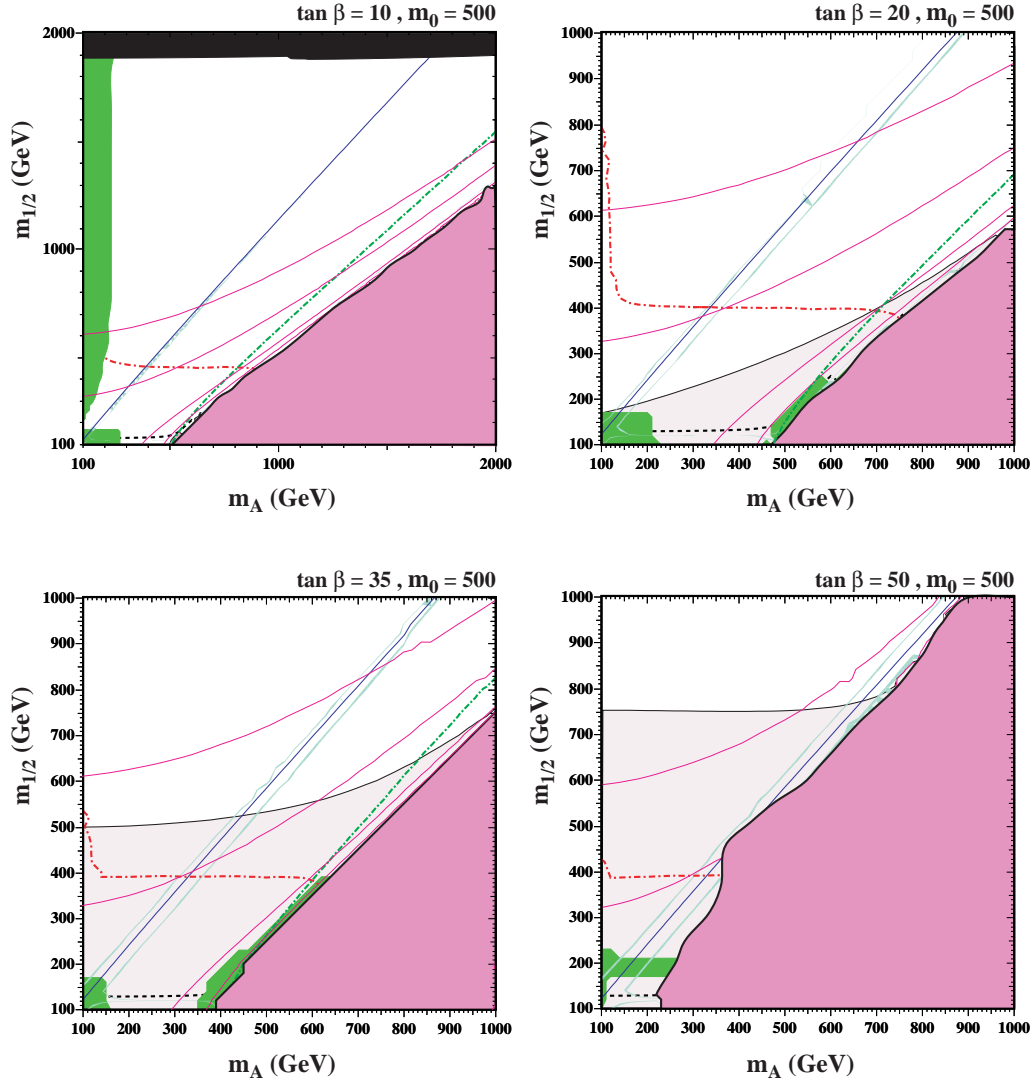


Figure 4: Examples of NUHM 1 ($m_A; m_{1=2}$) planes with $m_0 = 500$ GeV, $A_0 = 0$, $\mu > 0$, and $\tan \beta = 10, 20, 35$, and 50 in Panels (a), (b), (c), and (d), respectively. Constraints are displayed as in Figure 1.

In contrast to the CMSSM, in these particular NUHM 1 planes the constraint due to the branching ratio of $b \rightarrow s \gamma$ becomes insignificant at large $\tan \beta$. On the other hand, the region favored by $g_{\text{eff}} > 2$ expands such that a significant portion of the rapid-annihilation funnel falls within it, as well as the LEP constraint on the Higgs mass. In addition to the fixed rapid-annihilation funnel, in each panel of Fig. 4 there is a narrow WMAP strip close to the electroweak symmetry-breaking boundary. For $\tan \beta = 10$, portions of the funnel and this boundary strip are compatible with all these constraints, except $g_{\text{eff}} > 2$, for $m_{1=2} > 500$ GeV. When $\tan \beta = 20$, $m_{1=2} > 400$ GeV is allowed by the Higgs constraint,

and part of this boundary strip is also compatible with $g = 2$. When $\tan\beta = 35$, the region allowed by $g = 2$ extends to larger $m_{1=2}$, and parts of both the rapid-annihilation funnel and the boundary strip are compatible with it and with m_h .

In Fig. 5, we show NUHM 1 ($m_A; m_0$) planes with $m_{1=2} = 500$ GeV and $\tan\beta = 10, 20, 35$, and 50 in panels (a), (b), (c), and (d), respectively. Note that panel (a) of Fig. 5 is the same as panel (b) of Fig. 2. As $\tan\beta$ increases, we see that the boundary of the electroweak symmetry-breaking region moves to lower values of m_A , while the \sim -LSP region changes its shape, becoming less important at small m_A but more important at larger m_A . In contrast, the e -LSP region is fixed at very low m_0 as $\tan\beta$ is increased, becoming visible as the \sim -LSP region shifts, and it is bordered by a $g = 2$ coannihilation strip. The LEP Higgs constraint excludes only a narrow strip at small m_A , almost independent of m_0 , that narrows as $\tan\beta$ increases. The $b\bar{b}$ constraint is visible only for $\tan\beta = 10$, at small m_A . There is no region favoured by $g = 2$ when $\tan\beta = 10$, but this appears and expands as $\tan\beta$ increases. The CMSSM line arches up and outwards in each panel, following and gradually approaching the boundary of electroweak symmetry breaking.

The strip where the dark matter density falls within the WMAP range exhibits the familiar features of a rapid-annihilation funnel, which is near-vertical and straddles the blue line where $m = m_A = 2$, a coannihilation strip near the boundary of the charged LSP regions, and a strip near the boundary of the region where there is no electroweak symmetry breaking. This region is compatible with all the phenomenological constraints, including also $g = 2$ when $\tan\beta = 20$ or more. There are in general two intersections with the CMSSM line, corresponding to the coannihilation and fixed-point strips in the ($m_{1=2}; m_0$) planes for different values of $\tan\beta$. The rapid-annihilation funnel is in general at lower m_A than the CMSSM line, except for $\tan\beta = 50$. The analogous planes for larger $m_{1=2}$ would exhibit more intersections between the CMSSM line and the rapid-annihilation funnel.

According to previous studies [26,27], the LHC should find a signal of supersymmetry in the CMSSM scenario for $\tan\beta = 10$ with 10 fb^{-1} of integrated luminosity if $m_0 < 2000$ GeV for $m_{1=2} = 500$ GeV. Given the sensitivity of the sparticle spectrum to the value of $\tan\beta$, we estimate that the visible parts of the planes in Fig. 5 should be accessible to the LHC.

2.2 The NUHM 1 with μ as a Free Parameter

As discussed above, in the NUHM 1, one may choose either m_A or μ as the additional input to those of the CMSSM. In this subsection, we re-examine the parameter space, this time choosing μ as a free parameter. We begin, as in Section 2.1, with a comparison of the CMSSM ($m_{1=2}; m_0$) planes with NUHM 1 planes, now at fixed μ . In Fig. 6, we show in panel (a) the CMSSM plane (identical to panel (a) of Fig. 1), including the contours of constant m_A and μ of 300, 500, 1000, and 1500 GeV. Panels (b), (c), and (d) show the NUHM 1 planes with $m_{1=2} = 500, 1000, \text{ and } 1500$ GeV, respectively.

At first glance, the ($m_{1=2}; m_0$) planes with fixed μ have some similarities with those with fixed m_A . There are excluded regions at very low ($m_{1=2}; m_0$) where the pseudoscalar Higgs mass squared is negative, corresponding to the absence of electroweak symmetry breaking, surrounded by four contours of fixed $m_A = 300, 500, 1000, \text{ and } 1500$ GeV. At small values

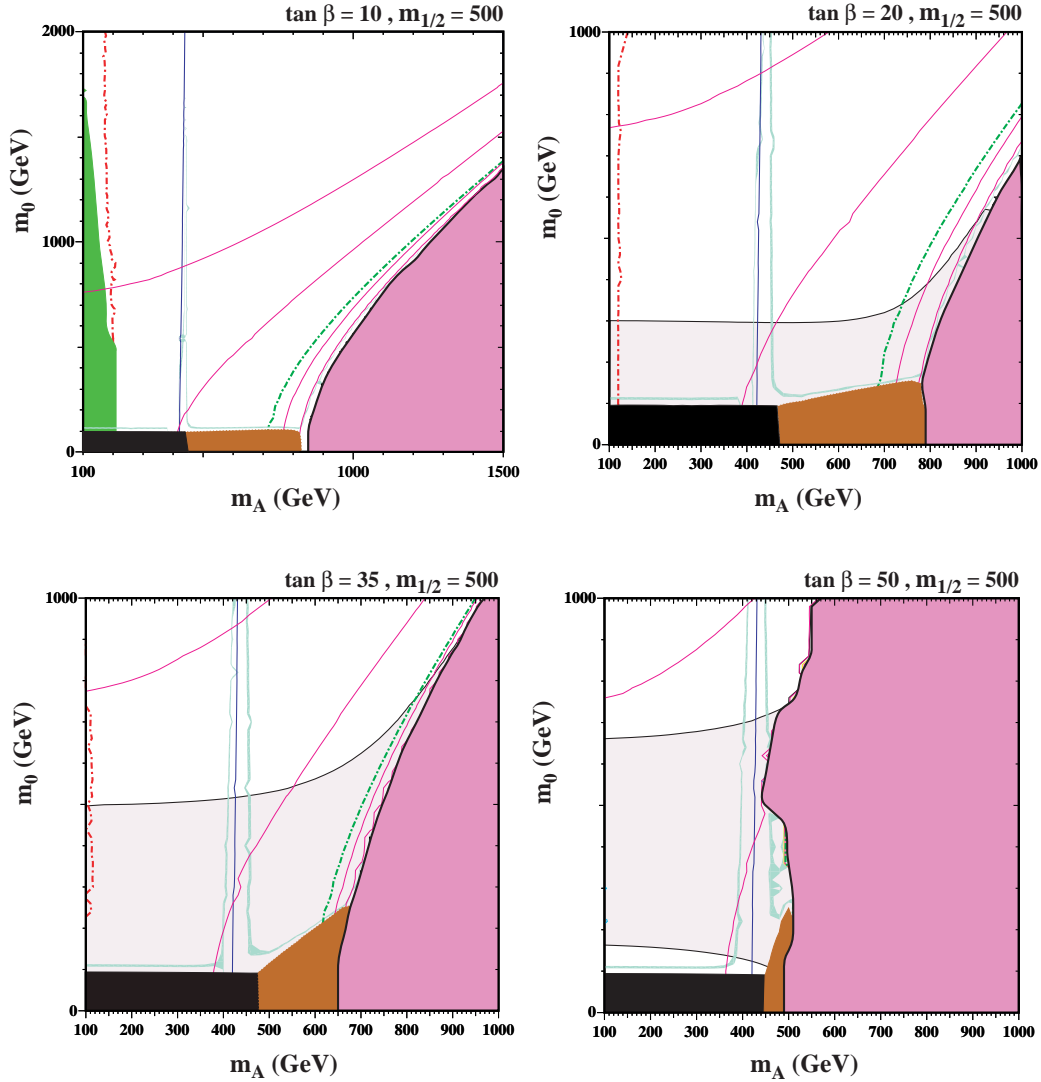


Figure 5: Examples of NUHM 1 ($m_A; m_0$) planes with $m_{1=2} = 500$ GeV, $A_0 = 0$, $\mu > 0$, and $\tan \beta = 10, 20, 35$, and 50 in Panels (a), (b), (c), and (d), respectively. Constraints are displayed as in Figure 1.

of m_0 , extending out to large $m_{1=2}$, there are excluded $\tilde{\nu}$ -LSP regions resembling those in the CMSSM. As usual, the LEP chargino and Higgs constraints exclude regions at small $m_{1=2}$, and $b \rightarrow s \gamma$ excludes strips near the electroweak symmetry-breaking boundaries for $m_{1=2} = 500; 1000$ GeV, shown in panels (b) and (c), respectively. We also see in these planes regions at low $m_{1=2}$ and m_0 that are favoured by $g_{\mu} = 2$.

There are three generic parts of the WMAP relic density strips in panels (b, c) and (d) of Fig. 6. There are coannihilation strips close to the $\tilde{\nu}$ - and e -LSP boundaries, and other strips close to the electroweak symmetry-breaking boundaries. Arching between these are

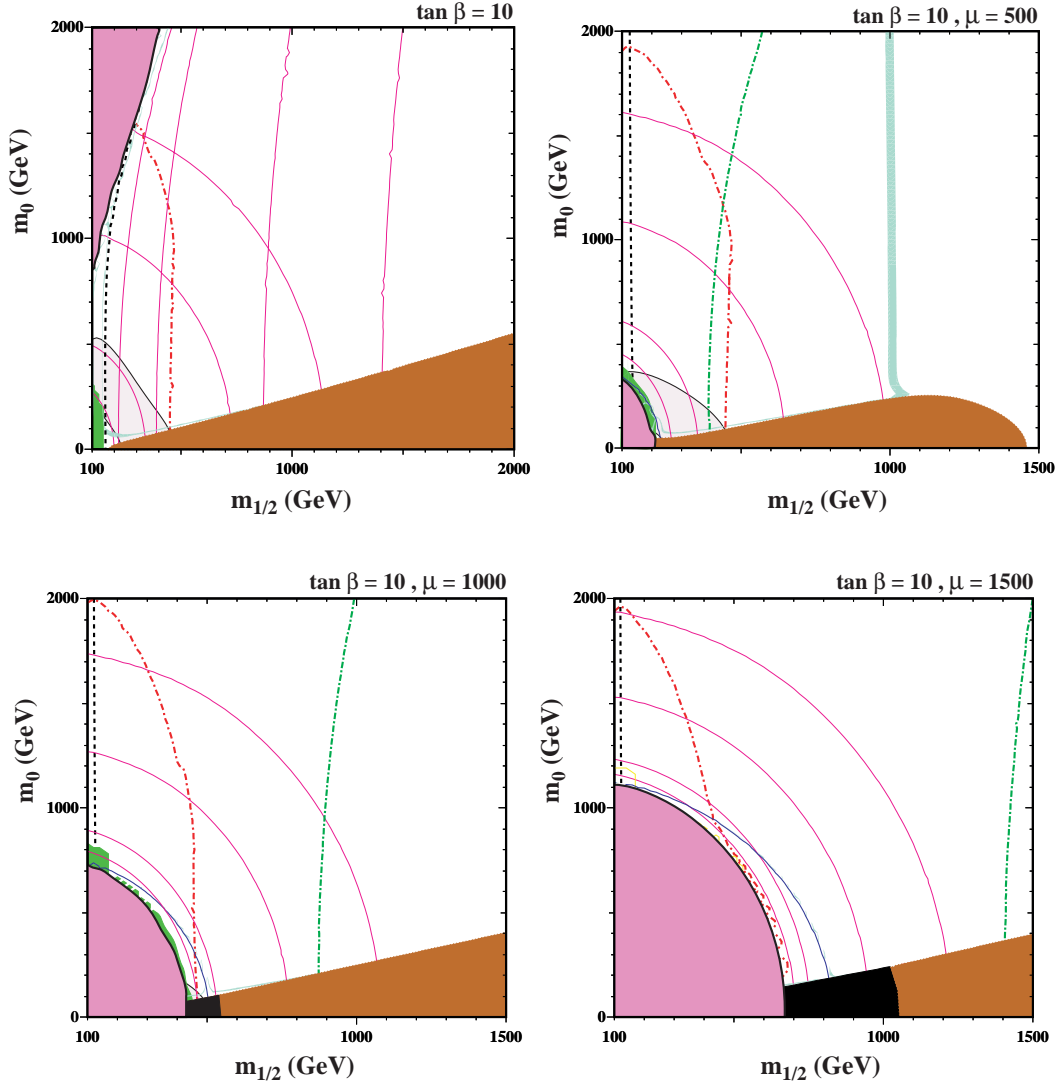


Figure 6: Panel (a) shows the $(m_{1/2}; m_0)$ plane for the CM SSM, with contours of m_A and of 300, 500, 1000, and 1500 GeV as described in the text. Panels (b), (c), and (d) show the NUHM 1 $(m_{1/2}; m_0)$ plane with $m_u = 500, 1000,$ and 1500 GeV, respectively. Constraints are displayed as in Figure 1.

curved rapid-annihilation funnels that appear at low m_A , with strips of good relic density forming the funnel walls. For $m_A = 1000$ GeV, the rapid-annihilation funnel is partially excluded by the branching ratio of $b \rightarrow s$ and even more so by m_h . Additionally, in panel (b) for $m_u = 500$ GeV, there is a fourth, near-vertical strip, where the relic density is brought down into the WMAP range because of the large mixing between the bino and Higgsino components in the LSP. For smaller $m_{1/2} < 500$ GeV, the LSP is almost pure bino, and the relic density is too large except in the narrow strips mentioned previously. This is the

opposite of what happens in the CM SSM, where the Higgsino fraction increases at smaller $m_{1=2}$ at large m_0 . On the other hand, for larger $m_{1=2} > 1000$ GeV, the LSP is almost pure Higgsino, and the relic density falls below the WMAP range³. At large m_0 in panel (b) of Fig. 6, it is only in the ‘crossover’ strip that the relic density falls within the WMAP range. Analogous near-vertical crossover strips are not visible in panels (c) and (d) of Fig. 6, but would in principle appear at larger $m_{1=2} = 2000; 3000$ GeV, respectively.

The CM SSM contour in each of panels (b, c) and (d) of Fig. 6 is a roughly vertical line, the position of which is determined by the value of m_A that one would find from the electroweak vacuum conditions in the standard CM SSM. Since the contours of constant m_A in these NUHM1 ($m_{1=2}; m_0$) planes look very similar to the corresponding contours in the CM SSM plane shown above, the CM SSM contours here in turn look qualitatively similar to contours of constant m_A in the CM SSM plane. The CM SSM lines are compatible with WMAP only in infinitesimal cuts across the coannihilation strips, missing all the excitement occurring elsewhere in the planes, namely the focus-point, rapid-annihilation and crossover strips.

In the NUHM1 ($m_{1=2}; m_0$) planes with fixed μ , the crossover strip and the rapid-annihilation funnel comprise regions of interest in addition to those commonly found in the CM SSM. Whereas the standard CM SSM regions will be fairly well-covered by the LHC, there are significant regions of the NUHM1 plane which may not be so easily accessed. For example, for $\mu = 500$ GeV, as shown in panel (b) of Fig. 6, the crossover strip runs at $m_{1=2} = 1000$ GeV from $m_0 = 260$ GeV, where it is terminated by the $\tilde{\nu}$ -LSP region, to well beyond 10 TeV, crossing the CM SSM contour at $m_0 = 3400$ GeV. Since the strip is roughly constant in $m_{1=2}$, at any point along it one finds $m_{\tilde{g}} = 430$ GeV and $m_{\tilde{u}} = 510$ GeV. The gluino mass is 2.2 to 2.3 TeV along this strip, which is expected to be within the LHC’s reach with just over 10 fb^{-1} of integrated luminosity [26,27]. If m_0 is low, then charged scalar particles may be accessible, with masses as low as 450 GeV. Above the CM SSM contour, however, all scalar particles have masses well above 3 TeV.

Tuning to panel (d), when $\mu = 1500$ GeV, we find a different situation. The rapid-annihilation funnel represents a cosmologically preferred region that occurs at moderate values of both $m_{1=2}$ and m_0 , in contrast to the CM SSM, where cosmologically-preferred regions generally occur at either small $m_{1=2}$ or small m_0 . Taking as an example the point $(m_{1=2}; m_0) = (640; 700)$ GeV, we find a rather light neutralino with $m_{\tilde{\chi}_1^0} = 275$ GeV. The chargino and pseudoscalar Higgs are somewhat heavier at 545 and 570 GeV, respectively, and charged scalars have masses of 735 GeV. This point is particularly interesting in that $m_{\tilde{g}} = 1480$ GeV, which should be accessible at the LHC with only 1 fb^{-1} of integrated luminosity. In the CM SSM, a gluino of 1480 GeV would imply either the coannihilation strip, where $m_{\tilde{\nu}} = 280$ GeV and $m_{\tilde{e}} = 285$ GeV, or the focus-point region, where charged scalars are much heavier. In the NUHM1, several particles may have masses below 1 TeV, and points on the rapid-annihilation strip should be distinguishable from points on the CM SSM coannihilation strip.

³It is also this change in the nature of the LSP that causes the boundary of the $\tilde{\nu}$ -LSP region to drop. Since the $\tilde{\nu}$ mass is affected only minimally by the value of μ , we find that $\tilde{\nu}$ -LSP region terminates at some value of $m_{1=2}$ related primarily to μ .

2.2.1 Fixed m_0

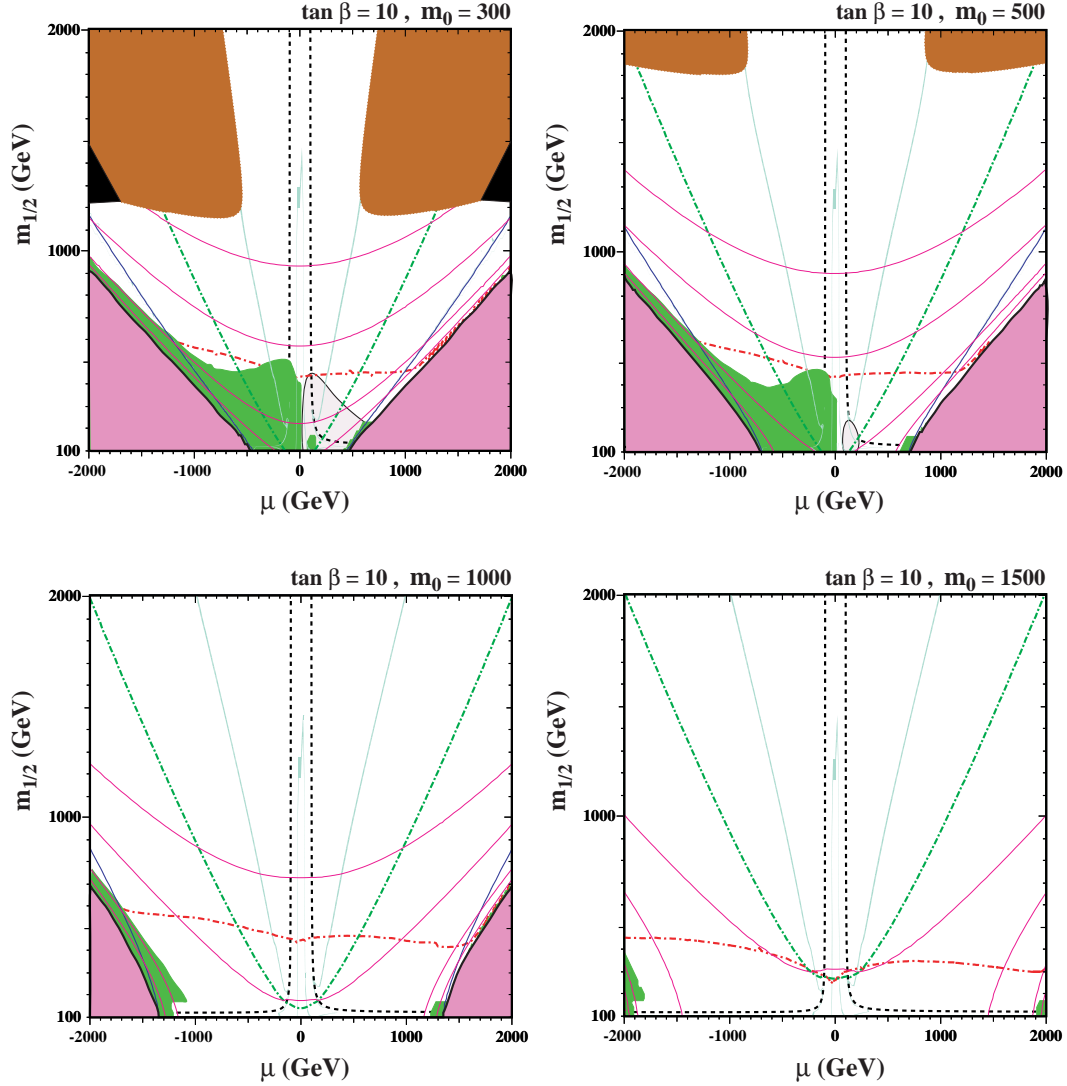


Figure 7: Examples of $(\mu; m_{1=2})$ planes with $\tan \beta = 10$, $A_0 = 0$, and $m_0 = 300, 500, 1000$, and 1500 GeV in Panels (a), (b), (c), and (d), respectively. Constraints are displayed as in Figure 1.

Analogously to the discussion in Section 2.1, alternative ways to view the parameter space are to fix either $m_{1=2}$ or m_0 and scan over μ . In Fig. 7, we show examples of $(\mu; m_{1=2})$ planes for fixed $m_0 = 300, 500, 1000$, and 1500 GeV in panels (a), (b), (c), and (d), respectively. For the first time, we display here both positive and negative values of μ . The unphysical regions excluded by not having electroweak symmetry breaking or by having a charged LSP cover a large part of the plane for $m_0 = 300$ GeV and recede out of the visible part of the plane as m_0 increases. Triangular regions in the lower right and left corners are forbidden because

the pseudoscalar Higgs mass-squared is negative. For fixed $\tan\beta$ and $m_{1=2}$, as m_0 increases, m_A increases slightly. As a result, the regions at small $m_{1=2}$ that had been excluded due to unphysical negative m_A^2 recede to larger j , dragging along the contours of constant $m_A = 300, 500, 1000, \text{ and } 1500 \text{ GeV}$. For $m_0 = 300 \text{ GeV}$, the upper right and left portions of the plane are forbidden because the stau is the LSP, though these regions move quickly to large $m_{1=2}$ as m_0 is increased, almost disappearing for $m_0 = 1000 \text{ GeV}$ and becoming invisible for larger m_0 . Bordering these regions of the plane (but away from the CMSSM contours) the selectron is lighter than the stau, forming a second region forbidden by the presence of a charged LSP.

In each panel, there is a strip at low j that is excluded by the LEP chargino constraint. Additionally, at low $m_{1=2}$ (slightly dependent on m_0), there is a region where the light Higgs mass falls below the LEP limit. Since m_h increases with $m_{1=2}$, the region below the Higgs mass contour is excluded, a constraint that is slightly stronger for $\tan\beta < 0$. The branching ratio of $b \rightarrow s \gamma$ constrains significantly more strongly the $\tan\beta < 0$ half of the plane, with the green area being excluded. However, the half-planes with $\tan\beta < 0$ are not all excluded in the NUHM1. The region favored by $g_{\text{eff}} > 2$ is found at small positive $\tan\beta$ and low $m_{1=2}$. However, it lies below the Higgs mass contour even at $m_0 = 300 \text{ GeV}$, and shrinks and then evaporates as m_0 is increased.

There are two cosmologically preferred regions in each plane⁴. Crossover regions form a long, narrow ‘Vee’ at relatively small $\tan\beta$, roughly proportional to $m_{1=2}$. The relic density of neutralinos is below the WMAP range inside the crossover ‘Vee’, and above the WMAP range at larger $\tan\beta$. In addition, rapid-annihilation funnels occur along diagonals that form a broader ‘Vee’ with slightly curved walls. These are very thin cosmologically preferred strips on either side of the blue lines where $2m_0 = m_A$, and the relic density is again below the WMAP range between the two strips of each rapid-annihilation funnel. We see that there are allowed regions of both the crossover strips and the rapid-annihilation funnels when $\tan\beta < 0$, as well as in the conventionally favoured case $\tan\beta > 0$. However, the latter also include lower values of $m_{1=2}$ where (in panel (a) for $m_0 = 300 \text{ GeV}$ and panel (b) for $m_0 = 500 \text{ GeV}$) the preferred range for $g_{\text{eff}} > 2$ may also be obtained.

Comparison with the CMSSM case shown in panel (a) of Fig. 6 yields insight into the appearance of the CMSSM contours in the NUHM1 planes of Fig. 7. Following a contour of constant m_0 , at low $m_{1=2}$ we begin in either the bulk region excluded by the LEP Higgs and/or chargino bounds and in the unphysical $\tan\beta < 0$ region. As we move to larger $m_{1=2}$, the sparticle masses and relic density generally increase, until one reaches the forbidden \sim -LSP region at very large $m_{1=2}$. Thus, the CMSSM contours in Fig. 7 begin at $\tan\beta = 0$ in a portion of the plane excluded by LEP, rising up to larger $m_{1=2}$ and $\tan\beta$. In the CMSSM, for $m_{1=2} = 2000 \text{ GeV}$, $j \approx 2000 \text{ GeV}$ and is sensitive to m_0 only at the level of $\approx 2\%$ for $300 \text{ GeV} < m_0 < 1500 \text{ GeV}$. It is well-known that in the CMSSM there is no rapid-annihilation funnel for $\tan\beta = 10$, so we do not expect the funnel regions in the NUHM1 to cross the CMSSM contours, as seen in all the panels of Fig. 7. At large m_0 , however, the CMSSM crossover WMAP strip appears at very low $\tan\beta$, so there is a crossing between each crossover WMAP strip and the CMSSM contour for $m_{1=2} \approx 1400 \text{ GeV}$.

⁴In addition, at low j there are regions disallowed by the LEP chargino constraint.

According to previous studies [26,27], the range of $m_{1=2}$ accessible to the LHC depends on the value of m_0 chosen, being roughly 900(900)(800)(700) GeV for the choices $m_0 = 300(500)(1000)(1500)$ GeV shown in Fig. 7. This implies that there are increasing portions of the crossover and rapid-annihilation strips that are likely to be inaccessible as m_0 increases from panels (a) and (b) to panels (c) and (d).

2.2.2 Fixed $m_{1=2}$

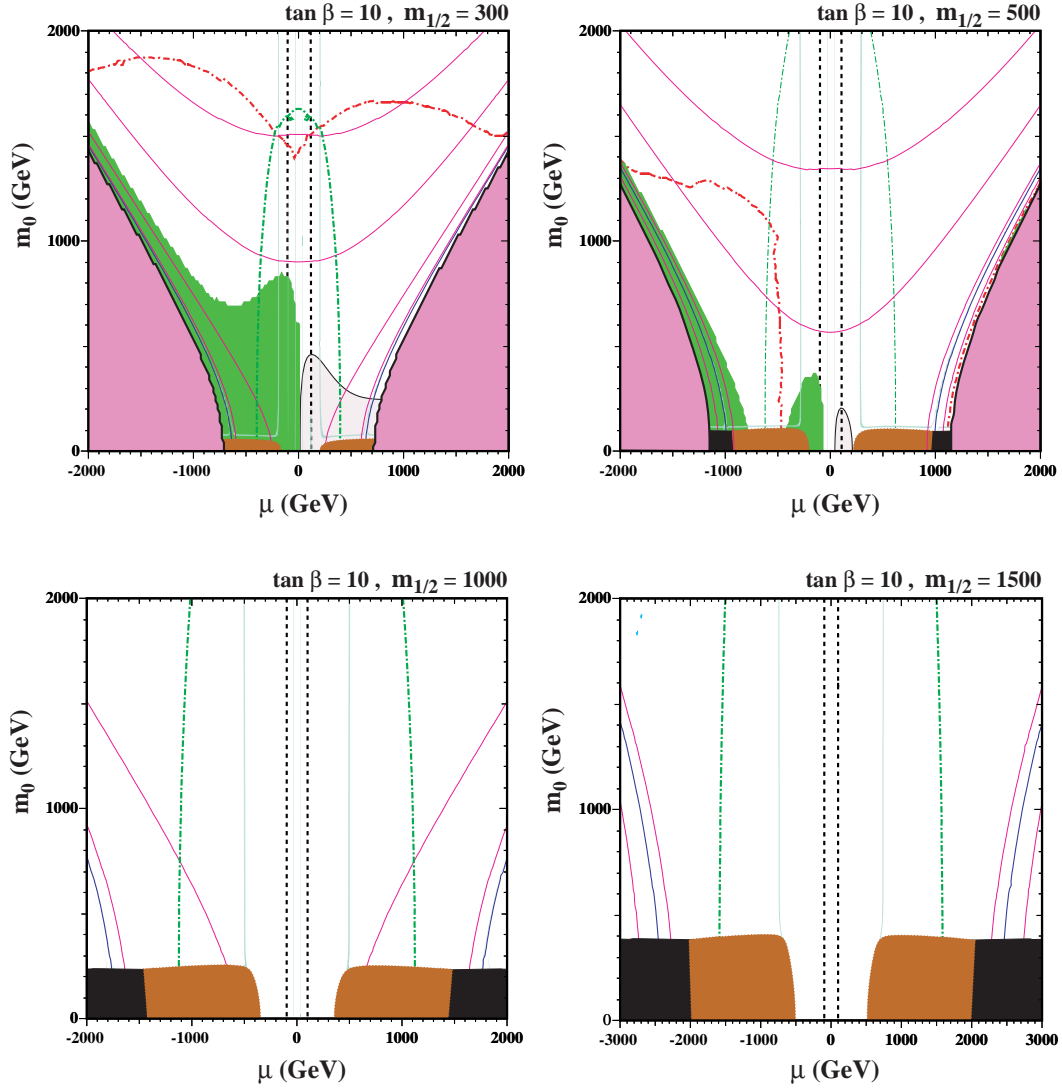


Figure 8: Examples of (μ, m_0) planes with $\tan \beta = 10$, $A_0 = 0$, and $m_{1=2} = 300, 500, 1000$, and 1500 GeV in Panels (a), (b), (c), and (d), respectively. Constraints are displayed as in Figure 1.

Fig. 8 shows NUHM 1 (μ, m_0) planes with $m_{1=2}$ fixed to be 300, 500, 1000, and 1500 GeV

in panels (a), (b), (c), and (d), respectively. Again, regions at large j_j excluded because there is no electroweak symmetry breaking (since $m_A^2 < 0$) are bordered by contours of constant m_A and parallel rapid-annihilation funnels. These regions recede and disappear for $m_{1=2} = 1000$ GeV. There are also excluded charged LSP regions at small m_0 , which expand as $m_{1=2}$ increases.

For $m_{1=2} = 300$ GeV, shown in panel (a) of Fig. 8, the LEP constraint on the Higgs mass excludes all of the plane below the contour at $m_0 = 1500$ GeV. The branching ratio of $b \rightarrow s$ also excludes a region with $\tan\beta < 0$ at lower m_0 . The chargino mass bound from LEP appears as vertical black dot-dashed lines at small j_j , and a region favored by $g_{21} > 2$ is visible at small positive $\tan\beta$. For $m_{1=2} = 500$ GeV, shown in panel (b), the Higgs constraint is weakened for $\tan\beta < 0$ and disappears for $\tan\beta > 0$, and the region favoured by $g_{21} > 2$ contracts. The Higgs and $b \rightarrow s$ constraints disappear completely when $m_{1=2} = 1000$ GeV.

The relic density of neutralinos may fall in the range favoured by WMAP in three regions of each $(\tan\beta; m_0)$ plane: along the rapid-annihilation funnels that straddle the blue lines where $m_A = 2m_{1=2}$, in the thin crossover strips that run outside and roughly parallel to the LEP chargino limits, and, at small m_0 , along coannihilation strips close to the excluded $\tilde{\nu}\tilde{\nu}$ - and $\tilde{e}\tilde{LSP}$ regions.

The CMSSM contours appear in these planes as parabolas, symmetric about $\tan\beta = 0$, with a peak height that increases dramatically with $m_{1=2}$. Since $m_{1=2}$ is constant in each of the planes, each half of each parabola may be regarded as tracing a line of constant $m_{1=2}$ in the standard CMSSM $(m_{1=2}; m_0)$ plane. When $m_{1=2} = 300$ GeV, at low m_0 one encounters the bulk region that is excluded by the Higgs constraint and (for $\tan\beta < 0$) the $b \rightarrow s$ constraint. The only points compatible with the dark matter and all other constraints are at $j_j = 100$ GeV and $m_0 = 1550$ GeV, barely satisfying the Higgs constraint. As m_0 increases, these CMSSM WMAP-compatible points move up to very large $m_0 > 2000$ GeV, a relic of the focus-point region in the familiar CMSSM $(m_{1=2}; m_0)$ plane. However, for 500 GeV $m_{1=2} = 900$ GeV we also encounter WMAP-compatible $\tilde{\nu}\tilde{\nu}$ -coannihilation points at the bottoms of the parabolae, which are compatible with all the other constraints (except the Higgs when $m_{1=2} = 500$ GeV and $\tan\beta < 0$). The CMSSM contours never cross the rapid-annihilation funnels for this value of $\tan\beta = 10$.

According to previous studies [26,27], the range of m_0 accessible to the LHC depends on the value of $m_{1=2}$ chosen, being above 2000 GeV for the choices $m_{1=2} = 300; 500$ GeV shown in panels (a) and (b) of Fig. 8. In the CMSSM, we do not expect to be able to probe supersymmetry with $m_{1=2} > 1000$ GeV, however in the NUHM1, there are regions of parameter space with heavy gauginos and much lighter scalars that may be accessible, specifically the lower portions of the crossover strips shown in panels (c) and (d).

2.2.3 Varying $\tan\beta$

We now consider the effect of varying $\tan\beta$, initially at fixed $m_0 = 500$ GeV. Panels (a), (b), (c), and (d) of Figure 9 show NUHM1 $(\tan\beta; m_{1=2})$ planes for $\tan\beta = 10, 20, 35,$ and 50 , respectively. In all panels, the requirement of electroweak symmetry breaking appears identically as a triangular excluded region at large j_j and low $m_{1=2}$. The $\tilde{\nu}\tilde{LSP}$ regions,

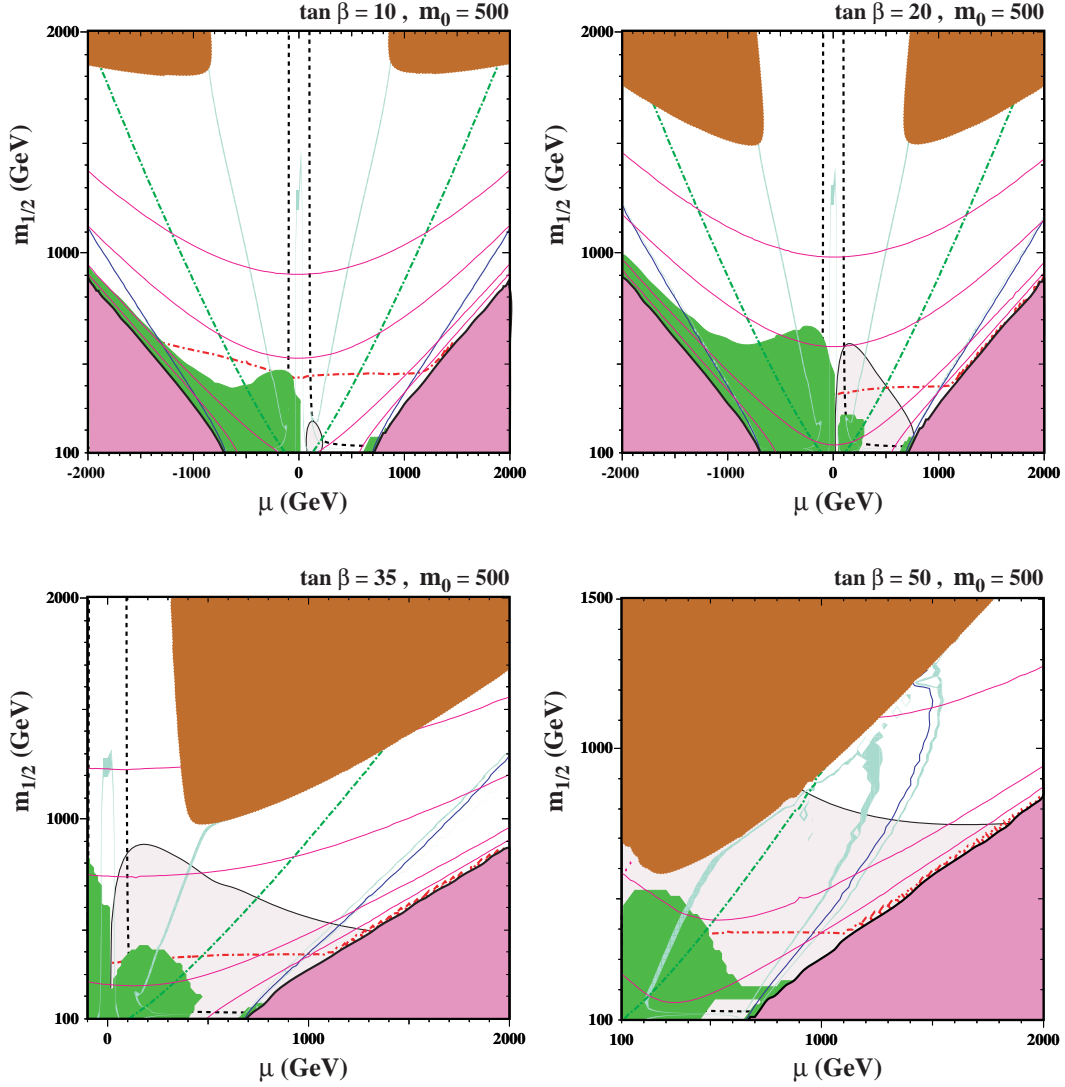


Figure 9: Examples of $(\mu; m_{1=2})$ planes with $m_0 = 500$ GeV, $A_0 = 0$, and $\tan \beta = 10, 20, 35$, and 50 in Panels (a), (b), (c), and (d), respectively. Constraints are displayed as in Figure 1.

while remaining similar in shape, become more prominent at large $\tan \beta$, as in the CMSSM. Focusing on $\mu > 0$, we see the constraint due to the branching ratio of $b \rightarrow s \gamma$ grows with $\tan \beta$, while the LEP Higgs constraint, for fixed m_0 , has little dependence on $\tan \beta$. In panels (c) and (d), we display only the $\mu > 0$ half of the plane for $\tan \beta = 35$ and 50 , since solutions are not reliably found for large $\tan \beta$ with $\mu < 0$.

In all panels, the crossover strips and the rapid-annihilation funnels are viable cosmologically preferred regions, both appearing as diagonals forming ‘Vees’ shapes in the planes. The CMSSM contours lie between the two ‘Vees,’ intersecting WMAP strips only in regions

excluded by collider constraints in panels (a) through (c). As $\tan \beta$ increases, the CM SSM contours shift to smaller j, j , while the rapid-annihilation funnel becomes more prominent and is deformed to lower j, j . At $\tan \beta = 50$, where a rapid-annihilation funnel is natural in the CM SSM, the coannihilation strip connects the crossover strip with the enlarged funnel region. For this fixed value of $m_0 = 500 \text{ GeV}$, the CM SSM contour does not intersect the rapid-annihilation funnel, however an intersection would occur for larger m_0 . At $\tan \beta = 50$, the region favoured by $g_{\text{eff}} > 2$ has expanded to encompass large regions of the plane where collider constraints are evaded and the dark matter density is in agreement with astrophysical measurements.

We recall that in the CM SSM, none of the regions of parameter space with $m_{1=2} \leq 1000 \text{ GeV}$ may be within the 10 fb^{-1} reach of the LHC [26,27] regardless of the value of $\tan \beta$. Extrapolating to the NUHM1, it is clear from Fig. 9 that portions of the crossover and rapid-annihilation strips, and possibly part of the $\tilde{\nu}$ -coannihilation strip at $\tan \beta = 50$, will be beyond the reach of the LHC. For comparison, in the CM SSM the corresponding $\tilde{\nu}$ -coannihilation strips would be accessible, but not portions of the focus-point and rapid-annihilation funnels.

Figure 10 shows examples of the $(\mu; m_0)$ plane at fixed $m_{1=2} = 500 \text{ GeV}$ for four choices of $\tan \beta$. Progressing from $\tan \beta = 10$ shown in panel (a), which is the same as panel (b) of Fig. 8, we see that, as $\tan \beta$ increases to 20 in panel (b), the regions excluded by the absence of electroweak symmetry breaking and the presence of a $\tilde{\nu}$ - or \tilde{e} -LSP are little changed⁵. However, the Higgs constraint essentially disappears, whereas the $b\tau$ constraint is much more aggressive at $\mu < 0$ and a larger region is favoured by $g_{\text{eff}} > 2$ at $\mu > 0$. A gain, in panels (c) and (d), we display only the $\mu > 0$ half of the plane.

The regions favoured by the dark matter density are crossover strips at $j, j \approx 300 \text{ GeV}$, rapid-annihilation funnels arching up close to the region excluded by the absence of electroweak symmetry breaking, and coannihilation strips close to the charged LSP regions. For $\tan \beta = 20$, separate $\tilde{\nu}$ - and \tilde{e} -coannihilation strips are easily discerned, separated by the rapid-annihilation funnel.

The CM SSM lines in the $(\mu; m_0)$ planes remain essentially unchanged as $\tan \beta$ increases. They always have intersections with the crossover strips at large $m_0 \approx 2000 \text{ GeV}$, for both signs of μ , and also intersect the $\tilde{\nu}$ -coannihilation strip for $\mu > 0$. This intersection is in the region favoured by $g_{\text{eff}} > 2$, whereas the corresponding intersection for $\mu < 0$ is excluded either by the LEP Higgs limit (for $\tan \beta = 10$) or $b\tau$ (for $\tan \beta = 20$). There are no intersections with the rapid-annihilation funnels or the \tilde{e} -coannihilation regions.

For the choice of $m_{1=2} = 500 \text{ GeV}$ made in Fig. 10, all the range of $m_0 \leq 2000 \text{ GeV}$ should be accessible to the LHC [26,27]. However, fewer of the heavier neutralinos, charginos and Higgs bosons would be detectable at larger values of μ (horizontal axis) and m_A (pink contours).

⁵Regions with tachyonic sfermions are found within the $\tilde{\nu}$ -LSP regions shown above for $\tan \beta = 35$.

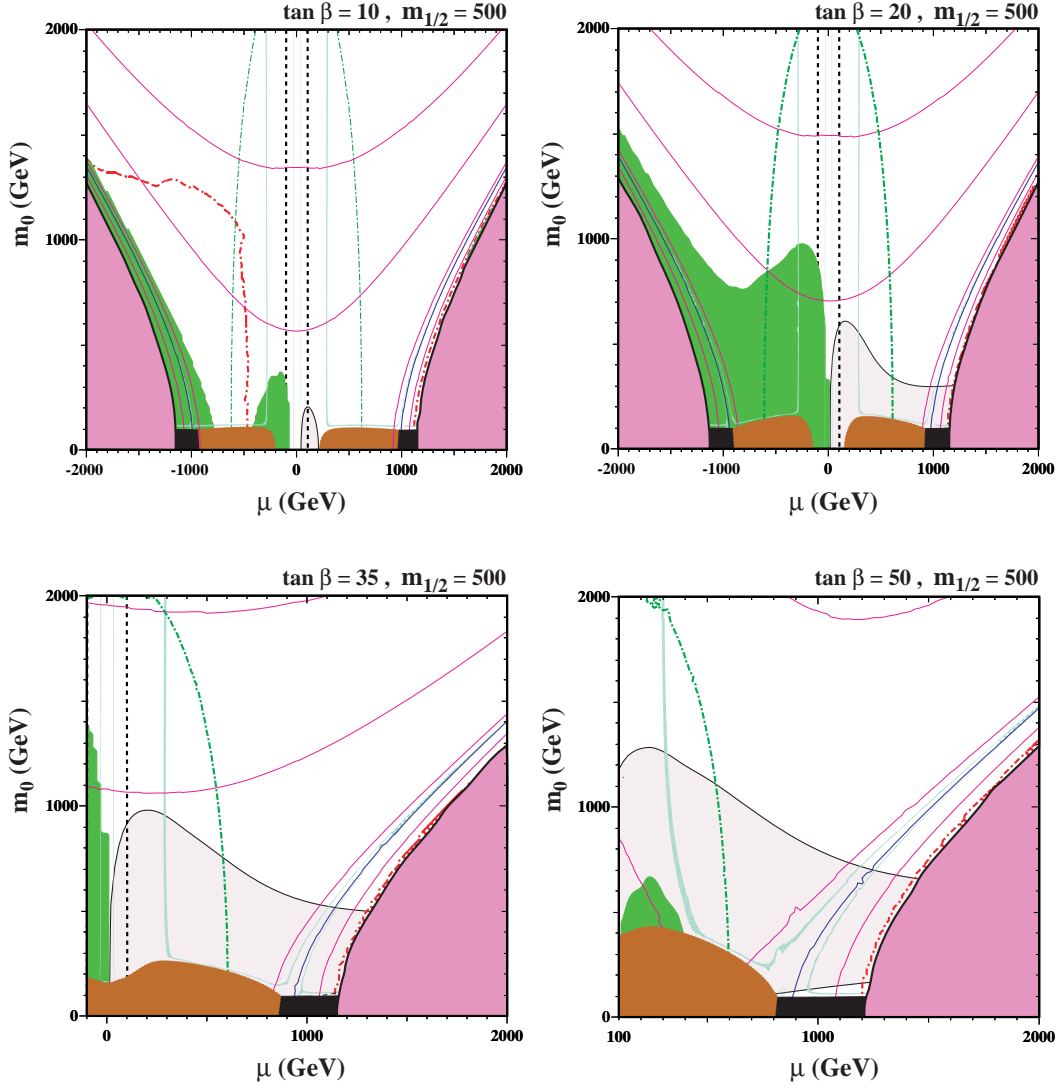


Figure 10: Examples of $(\mu; m_0)$ planes with $m_{1/2} = 500$ GeV, $A_0 = 0$, and $\tan \beta = 10, 20, 35$, and 50 in panels (a), (b), (c), and (d), respectively. Constraints are displayed as in Fig. 1.

3 From the NUHM 1 to the NUHM 2

Having situated the NUHM 1 relative to the CMSSM, we now discuss the extension to the NUHM 2, in which the soft supersymmetry-breaking contributions to both the Higgs scalar masses $m_{1,2}$ are regarded as free parameters. These two extra parameters imply that each point in a CMSSM $(m_{1/2}; m_0)$ plane can be ‘blown up’ into a $(\mu; m_A)$ plane, as displayed in Figs. 11, 12 and 13. Alternatively, one may display the NUHM 2 parameter space directly in $(m_1; m_2)$ planes, as we do in Figs. 14, 15 and 16. In the following, we use these ‘blow-ups’ to relate the NUHM 2 to the NUHM 1 and the CMSSM, noting that, in each plane, the NUHM 1

subspace may be represented as a line, and the CMSSM as one or two points on this line.

3.1 NUHM 2 ($\mu; m_A$) Planes

We start by considering the ($\mu; m_A$) ‘low-ups’ of points with the relatively small values $(m_{1=2}; m_0) = (300; 100)$ GeV, shown in Fig. 11. Panel (a) is for $\tan\beta = 10$. We see (brown) regions excluded because of a $\tilde{\chi}^0$ -LSP at small values of μ and m_A , and other regions at large values of μ and m_A excluded because either the $\tilde{\chi}^0$ (brown) or sneutrino (dark blue) is the LSP. Most of the half-plane with $\mu < 0$ is excluded by $b \rightarrow s$, and also a small region with small m_A and $\mu > 0$. The Higgs mass is slightly below the LEP constraint over the entire plane in all four panels of Fig. 11. In panel (a) compatibility with $g_{\mu\mu} = 2$ is found for $\mu > 0$. The dark matter density favoured by WMAP et al. is attained in narrow strips that stretch around the non-excluded regions. They feature a gaugino-Higgsino crossover at small μ and large m_A , sneutrino coannihilation at large μ and m_A , rapid-annihilation funnels at $m_A \approx 250$ GeV, and $\tilde{\chi}^0$ -coannihilation at small μ and m_A .

The NUHM 1 line is a symmetric parabola passing through $(\mu; m_A) = (700; 0)$ GeV and $(0; 550)$ GeV. For $\mu > 0$, this passes through the WMAP strip in three locations, once in the crossover strip at $m_A \approx 520$ GeV, and once on either side of the rapid-annihilation funnel at $m_A \approx 650$ GeV. These NUHM 1 WMAP-preferred region crossings are visible in the NUHM 1 planes, as well. For example, in panel (a) of Figure 3, where $m_{1=2} = 300$ GeV, by following $m_0 = 100$ GeV, one encounters precisely these three WMAP preferred strips, one at $m_A = 520$ GeV near the boundary of the region where electroweak symmetry breaking is not obtained, plus both walls of the rapid-annihilation funnel at lower m_A . The same crossings can be observed in the ($\mu; m_0$) plane when $m_{1=2}$ is fixed to be 300 GeV, by examining the $m_0 = 100$ GeV contour in a similar manner. On the other hand, the NUHM 1 line in the NUHM 2 plane completely misses the sneutrino coannihilation region at large μ and m_A , which is a new feature for the NUHM 2. In this case, the CMSSM point (marked by a + sign) is in a region interior to the WMAP strip, where the relic LSPs are overdense.

Turning now to the corresponding $(\mu; m_A)$ plane for $m_{1=2} = 300$ GeV, $m_0 = 100$ GeV and $\tan\beta = 20$, shown in panel (b) of Fig. 11, we see that the $\tilde{\chi}^0$ -LSP regions at low μ and m_A have expanded somewhat, and the $\tilde{\chi}^0$ -LSP regions at large μ have changed little, whereas the $\tilde{\chi}^0$ -LSP region has concentrated at large m_A . The $b \rightarrow s$ constraint is of reduced importance compared to panel (a), and $g_{\mu\mu} = 2$ now favours a region of small $\mu > 0$. The WMAP strip is qualitatively similar to that in panel (a), except that there are now separate $\tilde{\chi}^0$ - and $\tilde{\chi}^0$ -coannihilation regions at large m_A .

The NUHM 1 line follows closely the $\tilde{\chi}^0$ -coannihilation strip at low μ and m_A missing, in this case, both the crossover strip and the $\tilde{\chi}^0$ -coannihilation strip. In particular, the CMSSM points for both positive and negative μ would, with only minor adjustment, satisfy the WMAP constraint as well as the phenomenological constraints including $b \rightarrow s$. The CMSSM point with $\mu > 0$ also lies in the region favoured by $g_{\mu\mu} = 2$, as does a portion of the NUHM 1 strip extending from $m_A \approx 300$ to 500 GeV.

For larger values of $\tan\beta$, as seen in panels (c) and (d) of Fig. 11, the half-plane with $\mu < 0$ and a large part of the half-plane with $\mu > 0$ are excluded because the $\tilde{\chi}^0$ is the LSP.

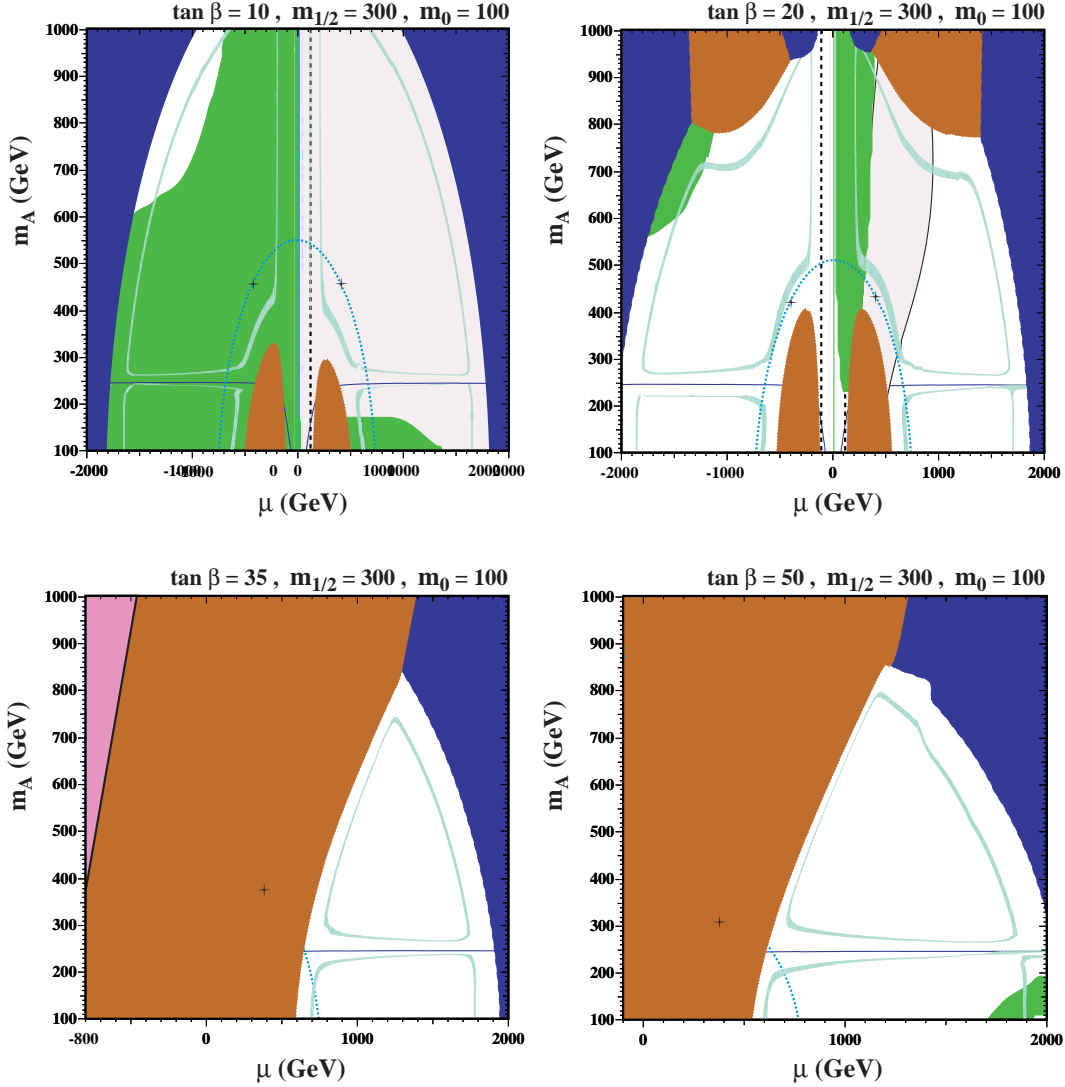


Figure 11: Examples of NUHM 2 (m_A vs μ) planes with $m_{1/2} = 300$ GeV, $m_0 = 100$ GeV, $A_0 = 0$, and $\tan \beta = 10, 20, 35,$ and 50 in panels (a), (b), (c), and (d), respectively. Constraints are displayed as in Fig. 1.

The \sim -LSP region at large $\mu > 0$ has also expanded, leaving only a (curved) triangle of allowed parameters at $\mu > 0$. The WMAP strip now consists of a \sim coannihilation strip and a \sim coannihilation strip, linked by a rapid-annihilation funnel. Since the values of $m_{1/2}$ and m_0 chosen for Fig. 11 are not large, all the WMAP-compatible points are accessible to the LHC [26,27], and several types of sfermions should be detectable. Some neutralinos, charginos and heavy Higgs bosons should also be detectable in the \sim coannihilation strip and the rapid-annihilation funnel, but this would be more difficult in the \sim coannihilation strip.

In both panels (c) and (d), only a small portion of the NUHM 1 line is allowed. It intersects the WMAP strip close to a junction between the $\tilde{\chi}^0$ coannihilation strip and the rapid-annihilation funnel. The CMSSM points in both panels are well within the excluded $\tilde{\chi}^0$ -LSP region, as could have been anticipated from the well-known fact that this region extends to higher m_0 (at fixed $m_{1=2}$) as $\tan\beta$ increases.

The configurations of the $(\mu; m_A)$ planes change significantly for $(m_{1=2}; m_0) = (500; 300)$ GeV, as seen in Fig. 12. The $\tilde{\chi}^0$ - and $\tilde{\chi}^0$ -LSP regions disappear completely in panels (a) and (b) for $\tan\beta = 10$ and 20, respectively. There is only a small excluded region in panel (c) for $\tan\beta = 35$, which grows naturally in panel (d) for $\tan\beta = 50$. Much of the $\mu < 0$ half-plane is excluded by $b \rightarrow s\gamma$ for $\tan\beta = 10$ and 20, but this constraint disappears for larger $\tan\beta$. The LEP Higgs constraint is not important in the regions allowed by $b \rightarrow s\gamma$. The $\mu > 0$ half-planes are favoured by $g_{\mu\mu} > 2$ for $\tan\beta \gtrsim 18$. The regions favoured by WMAP are rapid-annihilation funnels for all values of $\tan\beta$, crossover strips for $\tan\beta = 10; 20$ and 35, and $\tilde{\chi}^0$ coannihilation strips for $\tan\beta = 50$ and (nearly) for $\tan\beta = 35$.

The NUHM 1 lines are again (approximate) parabolas in all four panels. They intersect the WMAP strips in crossover and rapid-annihilation regions in panels (a, b) and (c), for $\tan\beta = 35$, and in the rapid-annihilation and $\tilde{\chi}^0$ coannihilation regions for $\tan\beta = 50$ in panel (d). We note that in panel (d) the approximate NUHM 1 parabola has shifted such that for some values of m_A there is no unique solution for μ .⁶ The CMSSM points are in strongly overdense regions in panels (a, b) and (c), but in the forbidden $\tilde{\chi}^0$ -LSP region of panel (d). However, this point is close to an allowed region where the relic density would be within the favoured range. Therefore, there are nearby CMSSM points with similar values of $m_{1=2}; m_0; \tan\beta; m_A$ and μ that are consistent with all the constraints. All these planes in Fig. 12 should be accessible to the LHC [26, 27], because of the moderate values chosen for $m_{1=2}$ and m_0 , but some heavier neutralinos, charginos and Higgs bosons would only be accessible for relatively small values of μ and m_A .

Finally, we present in Fig. 13 some $(\mu; m_A)$ planes for the choices $(m_{1=2}; m_0) = (500; 1000)$ GeV. Unlike the previous cases, these choices are in a region of the $(m_{1=2}; m_0)$ plane that is far from the coannihilation strip in the CMSSM. No parts of any of the planes are excluded by the absence of electroweak symmetry breaking or the presence of a charged LSP. We see explicitly in the panels (a, b) and (c) for $\tan\beta = 35$ that $b \rightarrow s\gamma$ again excludes most of the half-plane with $\mu < 0$. For $\tan\beta = 50$, shown in panel (d), reliable solutions are not found with $\mu < 0$. The LEP Higgs limit does not exclude a significant extra region of the $(\mu; m_A)$ plane in any of the panels. In panel (d) for $\tan\beta = 50$ there is a region at $\mu < 700$ GeV that is favoured by $g_{\mu\mu} > 2$, but not for the lower values of $\tan\beta$. In each of the panels, the region favoured by WMAP consists of a crossover strip at $\mu \approx 300$ GeV and a rapid-annihilation funnel with $400 \text{ GeV} < m_A < 450 \text{ GeV}$. These planes should also be accessible to the LHC [26, 27], though more luminosity would be required than in the previous cases because of the larger value of m_0 , in particular. This would also render more difficult the searches for some heavier neutralinos, charginos and Higgs bosons.

The NUHM 1 lines are again parabolas, reaching values of m_A that decrease from $\mu >$

⁶For this reason, the boundary of the region where there are no consistent solutions to the electroweak vacuum conditions appears augmented in the the NUHM 1, $\tan\beta = 50$ planes of Section 2.1.

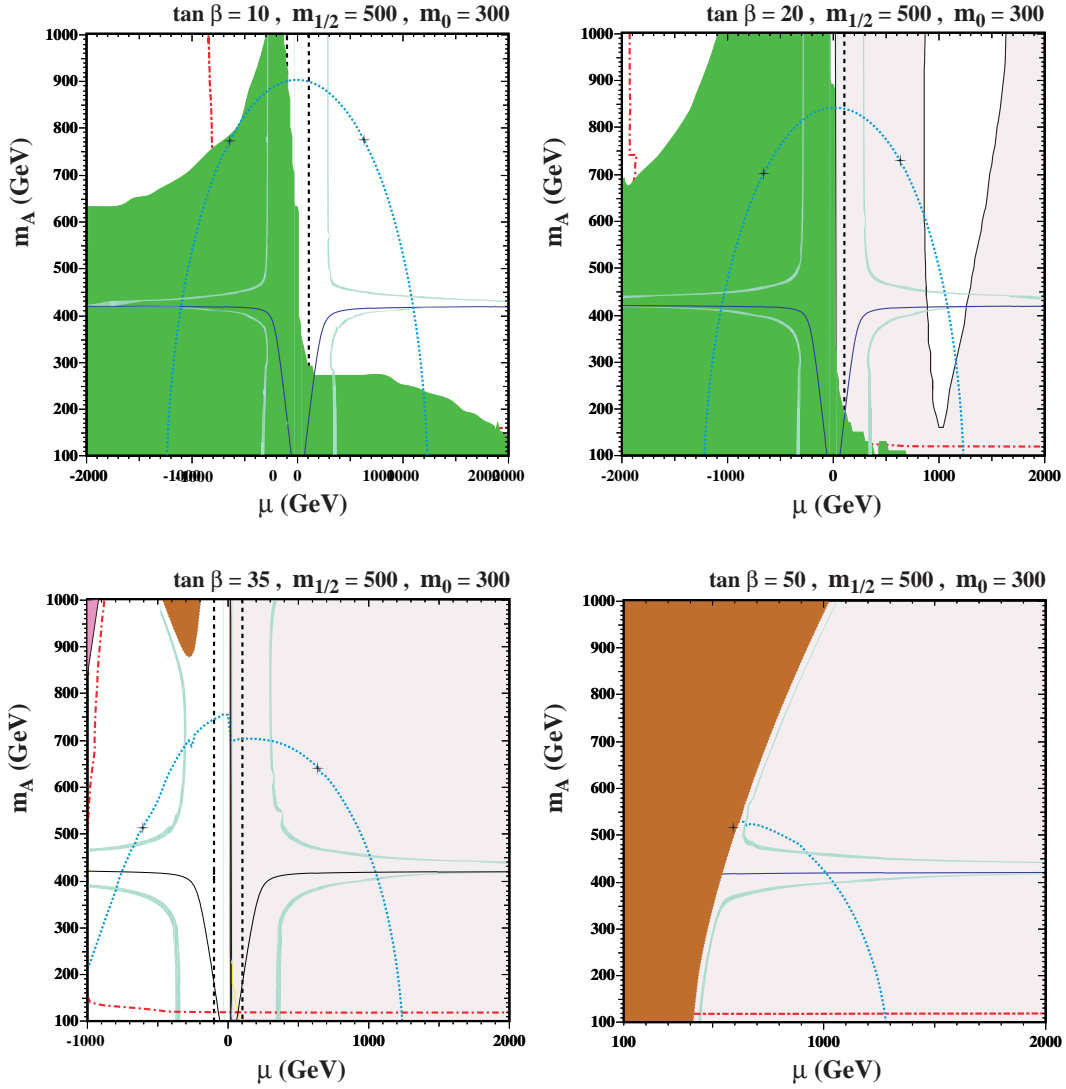


Figure 12: Examples of NUHM 2 (μ, m_A) planes with $m_{1/2} = 500$ GeV, $m_0 = 300$ GeV, $A_0 = 0$, and $\tan \beta = 10, 20, 35$, and 50 in panels (a), (b), (c), and (d), respectively. Constraints are displayed as in Fig. 1.

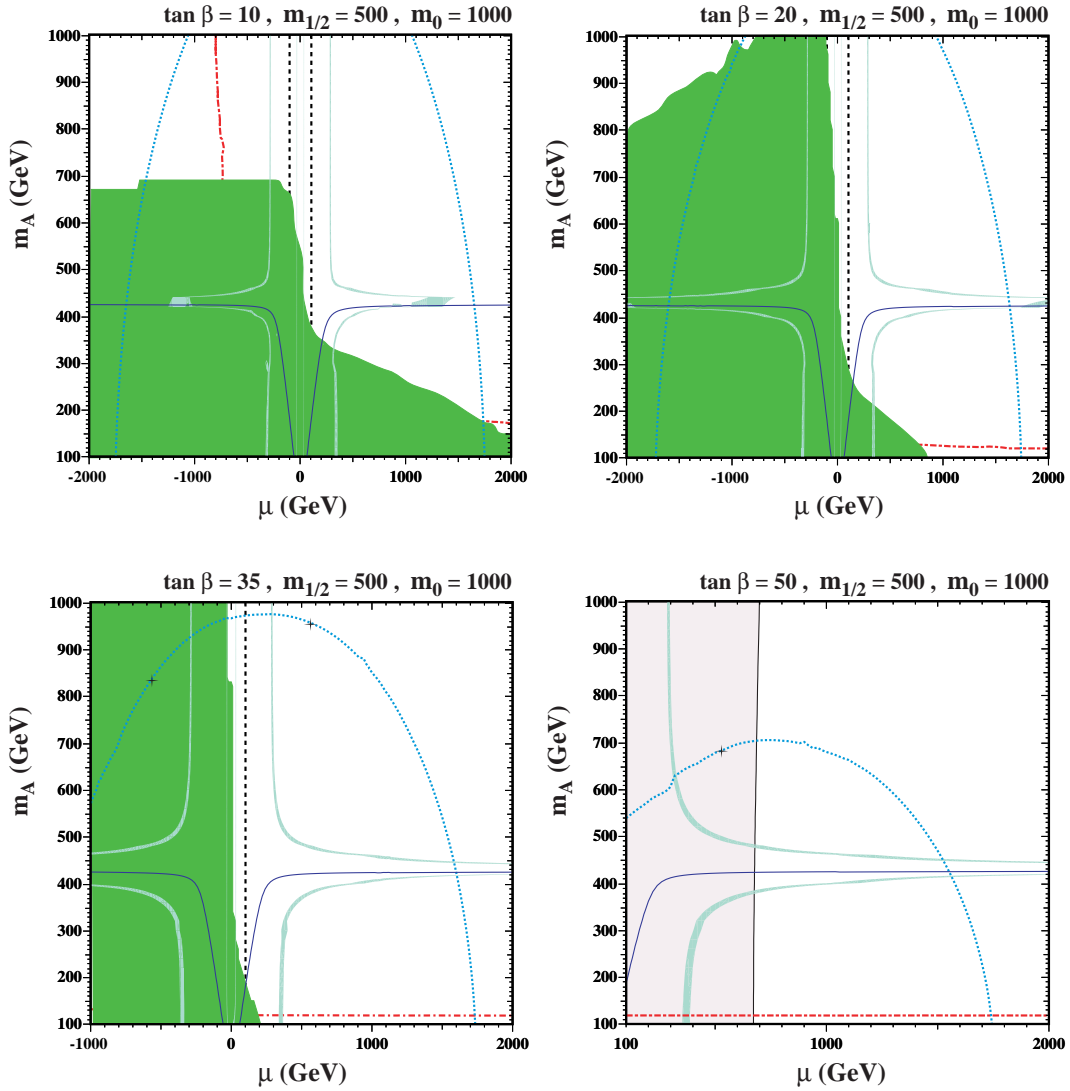


Figure 13: Examples of NUHM 2 (m_A) planes with $m_{1/2} = 500$ GeV, $m_0 = 1000$ GeV, $A_0 = 0$, and $\tan \beta = 10, 20, 35$, and 50 in panels (a), (b), (c), and (d), respectively. Constraints are displayed as in Fig. 1.

1000 GeV to 700 GeV as $\tan\beta$ increases, and becoming increasingly asymmetric in β . They intersect the WMAP regions in both the rapid-annihilation strips and the crossover strips (the latter at $m_A > 1000$ GeV for $\tan\beta < 20$). Thus, the NUHM 1 lines do sample both the WMAP possibilities in these NUHM 2 planes. On the other hand, the CMSSM points are always in strongly overdense regions of the $(m_{1=2}; m_A)$ planes.

As the GUT-scale values of the gaugino and scalar masses are fixed in the NUHM 2 planes in Figures 11–13 (as well as Figures 14–16 in the next subsection), the sparticle spectrum does not vary much over any individual panel, the primary exceptions being the Higgs masses. What is novel in the NUHM 2 is that there are allowed regions of the NUHM 2 parameter space with very low $(m_{1=2}; m_0)$, leading to sparticle masses below what would be expected in the CMSSM. Alternatively, inspection of $(m_{1=2}; m_A)$ planes for large $(m_{1=2}; m_0)$ would show that there are indeed cosmologically preferred strips that evade all collider constraints and have very heavy sparticles.

3.2 NUHM 2 $(m_{1=2}; m_2)$ Planes

We now present a novel analysis of the NUHM 2, based directly on the input non-universal soft supersymmetry-breaking parameters, $m_{1=2}$ and m_2 , for the same choices of $m_{1=2}$ and m_0 as were used in the previous subsection.

Fig. 14 shows a selection of $(m_{1=2}; m_2)$ planes for the same values $(m_{1=2}; m_0) = (300; 100)$ GeV as in Fig. 11. We notice immediately that large negative values of m_1 and positive values of m_2 are excluded by the electroweak symmetry-breaking requirement, and regions of positive m_1 and negative m_2 are excluded because the $\tilde{\nu}$ or \tilde{e} is the LSP. There are also $\tilde{\nu}$ -LSP excluded regions in the second quadrant of panels (a) and (b), for $\tan\beta = 10$ and 20. The slepton-LSP constraints become much stronger as $\tan\beta$ increases, with the effect that the allowed region of parameter space is pushed to values of $m_{1,2}^2 \gg 0$, far away from values where $m_{1,2} = m_0 = 0$ (1). The dashed blue diagonal lines in panels (a) and (b) are the NUHM 1 lines where $m_1 = m_2$, and the CMSSM points are found at $m_1 = m_2 = m_0$.

As in Fig. 11, the Higgs mass is slightly below the LEP constraint over the entire plane in all four panels of Fig. 14. The LEP chargino constraint runs close to the upper boundaries of the allowed regions in panels (a) and (b) of Fig. 14. The $b \rightarrow s$ constraint is visible only in panel (b), for $\tan\beta = 20$, where it excludes a large part of the first quadrant. Likewise, the region favoured for $g \rightarrow 2$ is also visible only in panels (a) and (b), where it covers most of the allowed part of the $(m_{1=2}; m_2)$ plane.

It is a common feature of all the panels that the WMAP strip skirts the boundaries of the allowed region. In panels (a) for $\tan\beta = 10$ and (b) for $\tan\beta = 20$, it comprises a crossover strip at the top and, combined with a rapid-annihilation funnel in the bottom left corner, a $\tilde{\nu}$ coannihilation strip on the left side, and a $\tilde{\nu}$ coannihilation strip (in (a)) and a \tilde{e} coannihilation strip (in (b)) on the right side. In panels (c) for $\tan\beta = 35$ and (d) for $\tan\beta = 50$, it comprises a crossover strip/rapid-annihilation funnel on the left side and a coannihilation strip on the right side.

⁷A gain, this leads to a lack of unique solutions for β for some choices of m_A, m_0 , and $m_{1=2}$ with $\tan\beta = 50$.

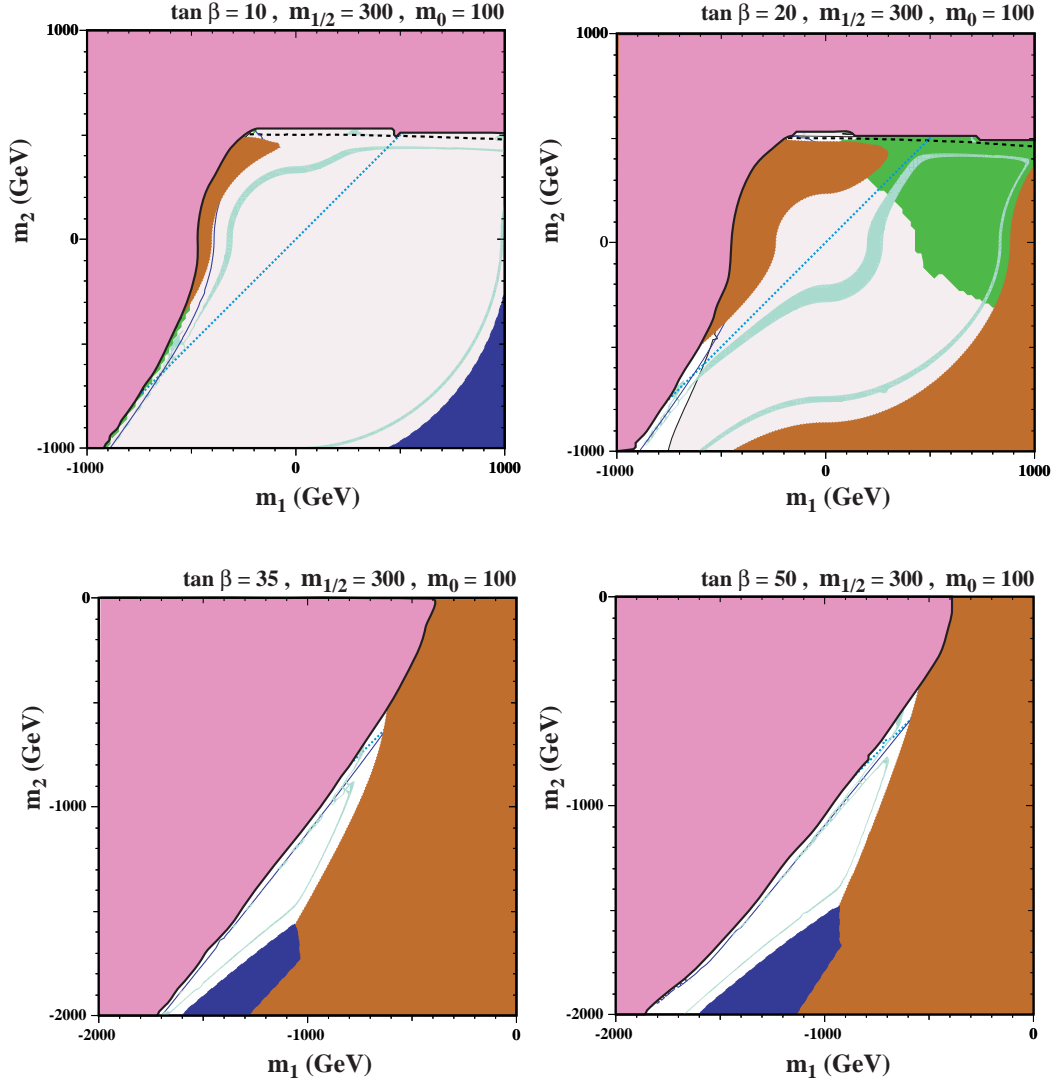


Figure 14: Examples of NUHM 2 (m_1, m_2) planes with $m_{1=2} = 300$ GeV, $m_0 = 100$ GeV, $A_0 = 0$, and $\tan \beta = 10, 20, 35$, and 50 in panels (a), (b), (c), and (d), respectively. The sign in the axes labels refer to the sign of $m_{1/2}^2$. Constraints are displayed as in Fig. 1.

In panel (a), the NUHM 1 line intersects the WMAP strip in the crossover strip in the first quadrant and in the crossover/rapid-annihilation strip in the third quadrant. We note that both these regions have the common value of $\ln \Omega_{1,2} h^2 = m_0$. Most of the rest of the NUHM 1 line has excessive relic density. On the other hand, in panel (b), the relic density lies below the WMAP range along all the NUHM 1 line, except in the third quadrant. The CMSSM points in these two panels have relic densities that are too large, in panel (a) for $\tan \beta = 10$, or too small, in panel (b) for $\tan \beta = 20$. The NUHM 1 lines lie mostly in regions which are excluded and the CMSSM points are in the disallowed regions of panels (c) and (d).

Analogous $(m_1; m_2)$ planes for the choices $(m_{1=2}; m_0) = (500; 300)$ GeV are shown in Fig. 15. In this case, the electroweak symmetry-breaking condition excludes strips at large positive m_2 and large negative m_1 . The condition for the absence of a $\tilde{\chi}^0$ LSP forbids a region with large $m_1 > 0$ for $\tan \beta = 50$, as shown in panel (d). The LEP chargino constraint excludes a narrow strip close to the boundary in the first and second quadrants in panels (a, b) and (c), i.e., for $\tan \beta < 35$, and the Higgs constraint excludes a narrow strip along the boundary in the second and third quadrants in all panels. The $b \rightarrow s$ constraint is absent except for $\tan \beta = 10$, whilst there are large regions favoured by $g_{\mu\mu} < 2$ for $\tan \beta = 20, 35$, and 50, but not for $\tan \beta = 10$.

The rapid-annihilation funnel evolves in an interesting way as $\tan \beta$ increases. After starting close to the left boundary for $\tan \beta = 10$, it moves out into the allowed region as $\tan \beta$ increases, and becomes increasingly serpentine. The two sides of the funnel run almost parallel for $\tan \beta < 35$, with the right side extended by a crossover strip along the top boundary for $\tan \beta > 35$. On the other hand, for $\tan \beta = 50$, the right boundary of the rapid-annihilation funnel expands and evolves into a $\tilde{\chi}^0$ coannihilation strip.

In panels (a, b) and (c) for $\tan \beta < 35$, the NUHM 1 lines intersect the WMAP region in the crossover strip at large positive m_1 and m_2 , and in the rapid-annihilation funnel at large negative m_1 and m_2 . These intersections lie far from the CMSSM point, which is in an overdense region. On the other hand, for $\tan \beta = 50$ in panel (d), the CMSSM point lies very close to a WMAP strip, in an underdense region.

In the case $(m_{1=2}; m_0) = (500; 1000)$ GeV shown in Fig. 16, the electroweak symmetry-breaking condition again excludes large portions of the plane that expand somewhat as $\tan \beta$ is increased⁸. The requirement that the LSP be neutral does not constrain the parameter space. The $b \rightarrow s$ constraint excludes only a narrow strip along the left boundary of panel (a), and the LEP Higgs constraint also excludes only narrow boundary regions in all four panels.

The only WMAP regions are confined to rapid-annihilation funnels, supplemented in panel (d) for $\tan \beta = 50$ by an extension to a crossover strip. Imitating its behaviour in Fig. 15, the funnel is again quite serpentine. The NUHM 1 line does not intersect this funnel, but does cross the crossover strip in panel (d). Thus, the NUHM 1 lines lie almost entirely in overdense regions, and the CMSSM points are all overdense.

⁸Note that the ranges of m_1 and m_2 displayed in Fig. 16 differ from panel to panel.

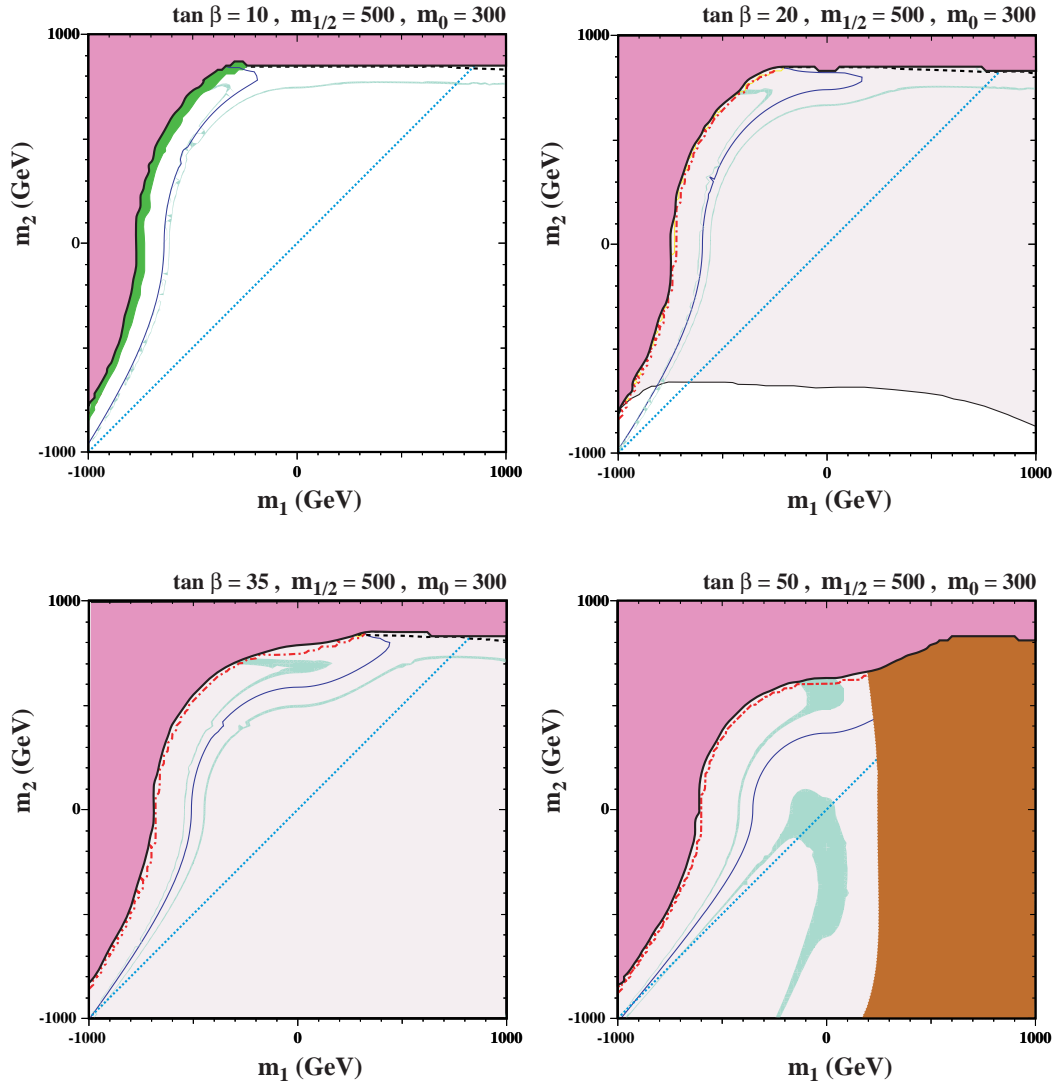


Figure 15: Examples of NUHM 2 (m_1, m_2) planes with $m_{1/2} = 500$ GeV, $m_0 = 300$ GeV, $A_0 = 0$, and $\tan \beta = 10, 20, 35$, and 50 in panels (a), (b), (c), and (d), respectively. Constraints are displayed as in Fig. 1.

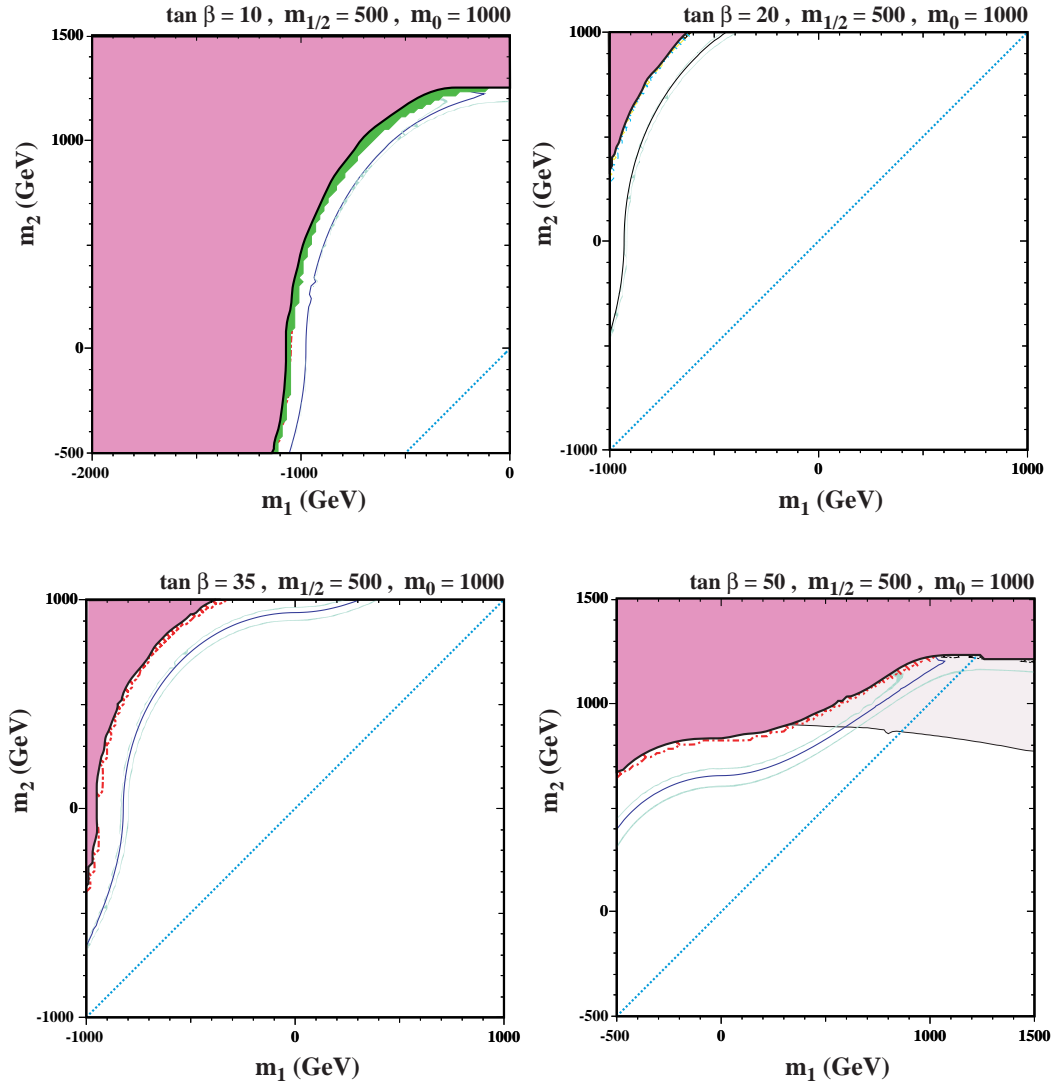


Figure 16: Examples of NUHM 2 $(m_1; m_2)$ planes with $m_{1/2} = 500$ GeV, $m_0 = 1000$ GeV, $A_0 = 0$, and $\tan \beta = 10, 20, 35,$ and 50 in panels (a), (b), (c), and (d), respectively. Constraints are displayed as in Fig. 1.

4 Conclusions

We have studied in this paper how the CMSSM parameter space may be embedded successively in the larger NUHM1 and NUHM2 parameter spaces. We find several qualitatively new features in making these generalizations.

One new feature of the NUHM1 is that the allowed domain is restricted in places by the requirement that the LSP not be a selectron, a possibility that does not arise within the CMSSM. Another feature of the NUHM1 is that there may be funnels of parameter space where rapid annihilation through direct-channel Higgs poles extends the WMAP-compatible part of parameter space to large m_0 and/or $m_{1=2}$ even for $\tan\beta = 10$, whereas this feature appears only at much larger $\tan\beta$ in the CMSSM. This is because m_A can be regarded as a free parameter within the NUHM1, whereas it is calculable in terms of $m_{1=2}, m_0, A_0$ and $\tan\beta$ in the CMSSM. Other features of the dark matter density in the NUHM1 include the possibility that neutralino-selectron coannihilation may be important close to the forbidden selectron-LSP region, and the possibility that the relic density may be suppressed into the WMAP-compatible range in regions where the neutralino composition crosses over from being mainly bino to mainly Higgsino.

Additional new features appear in the further generalization to the NUHM2. For example, the allowed region of parameter space is partly restricted by the requirement that the LSP not be a sneutrino. Near this boundary, neutralino-sneutrino coannihilation can be important for bringing the relic neutralino density into the WMAP-compatible range.

One of the novel features of this study has been the presentation of constraints in the (m_1, m_2) plane for certain fixed values of the other parameters. It is striking that the relic density requirement, in particular, often favours values of the parameters where both $|m_{1,2}| \approx m_0$, and they are far from being equal to each other. There is no hint that the NUHM1 subspace is favoured within the larger NUHM2 space, and still less suggestion that the smaller CMSSM subspace is favoured in any way.

One of the prime motivations for this study has been to understand to what extent the good coverage of the WMAP-compatible CMSSM region by the LHC can be generalized to the NUHM1 and NUHM2. In the CMSSM, the LHC covers the stau coannihilation region, but not completely the focus-point region (which can be regarded as an example of a bino/Higgsino crossover), nor the rapid-annihilation funnel that appears at large $\tan\beta$. In the NUHM1, the appearance of selectron coannihilation does not add to the woes of the LHC. However, the rapid-annihilation funnels extending to large m_0 and/or $m_{1=2}$ may be problematic for the LHC, as may the crossover strips that may also appear at relatively large $m_{1=2}$ and extend to large m_0 . However, it remains the case that the LHC can cover a large fraction of the NUHM1 and NUHM2 parameter spaces. If the LHC does indeed discover supersymmetry, a key check whether the scalar masses are universal, in addition to sfermion mass measurements, will be to determine the values of m_A and $\tan\beta$, and to explore whether they are compatible with the values required by the electroweak vacuum conditions within the CMSSM. This would be possible, e.g., by measuring the masses of heavier Higgs bosons, neutralinos and charginos. This should be possible if $m_{1=2}$ and m_0 are not too large, but such a study lies beyond the scope of this paper.

Acknowledgments

The work of K.A.O. and P.S. was supported in part by DOE grant DE-FG02-94ER-40823. P.S. would like to acknowledge support from the Doctoral Dissertation Fellowship Program at the University of Minnesota.

References

- [1] M. Drees and M. M. Nojiri, *Phys. Rev. D* 47 (1993) 376 [arXiv:hep-ph/9207234]; H. Baer and M. Brhlik, *Phys. Rev. D* 53, 597 (1996) [arXiv:hep-ph/9508321]; H. Baer and M. Brhlik, *Phys. Rev. D* 57, 567 (1998) [arXiv:hep-ph/9706509]; H. Baer, M. Brhlik, M. A. Diaz, J. Ferrandis, P. Mercadante, P. Quintana and X. Tata, *Phys. Rev. D* 63 (2001) 015007 [arXiv:hep-ph/0005027]; J. R. Ellis, T. Falk, G. Ganis, K. A. Olive and M. Srednicki, *Phys. Lett. B* 510 (2001) 236 [arXiv:hep-ph/0102098]; A. B. Lahanas, D. V. Nanopoulos and V. C. Spanos, *Mod. Phys. Lett. A* 16 (2001) 1229 [arXiv:hep-ph/0009065].
- [2] J. R. Ellis, T. Falk, K. A. Olive and M. Schmitt, *Phys. Lett. B* 388 (1996) 97 [arXiv:hep-ph/9607292]; *Phys. Lett. B* 413 (1997) 355 [arXiv:hep-ph/9705444]; J. R. Ellis, T. Falk, G. Ganis, K. A. Olive and M. Schmitt, *Phys. Rev. D* 58 (1998) 095002 [arXiv:hep-ph/9801445]; V. D. Barger and C. Kao, *Phys. Rev. D* 57 (1998) 3131 [arXiv:hep-ph/9704403]; J. R. Ellis, T. Falk, G. Ganis and K. A. Olive, *Phys. Rev. D* 62 (2000) 075010 [arXiv:hep-ph/0004169]; V. D. Barger and C. Kao, *Phys. Lett. B* 518 (2001) 117 [arXiv:hep-ph/0106189]; L. Roszkowski, R. Ruiz de Austri and T. Nihei, *JHEP* 0108 (2001) 024 [arXiv:hep-ph/0106334]; A. B. Lahanas and V. C. Spanos, *Eur. Phys. J. C* 23 (2002) 185 [arXiv:hep-ph/0106345]; A. Djouadi, M. Drees and J. L. Kneur, *JHEP* 0108 (2001) 055 [arXiv:hep-ph/0107316]; U. Chattopadhyay, A. Corsetti and P. Nath, *Phys. Rev. D* 66 (2002) 035003 [arXiv:hep-ph/0201001]; J. R. Ellis, K. A. Olive and Y. Santoso, *New Jour. Phys.* 4 (2002) 32 [arXiv:hep-ph/0202110]; H. Baer, C. Balazs, A. Belyaev, J. K. Mizukoshi, X. Tata and Y. Wang, *JHEP* 0207 (2002) 050 [arXiv:hep-ph/0205325]; R. A. Mowitt and B. Dutta, arXiv:hep-ph/0211417.
- [3] J. R. Ellis, K. A. Olive and P. Sandick, *Phys. Lett. B* 642 (2006) 389 [arXiv:hep-ph/0607002]; *JHEP* 0706 (2007) 079 [arXiv:0704.3446 [hep-ph]]; arXiv:0801.1651 [hep-ph].
- [4] K. Choi, A. Falkowski, H. P. Nilles and M. Olechowski, *Nucl. Phys. B* 718 (2005) 113 [arXiv:hep-th/0503216]. K. Choi, K. S. Jeong and K. I. Okumura, *JHEP* 0509 (2005) 039 [arXiv:hep-ph/0504037]; M. Endo, M. Yamaguchi and K. Yoshioka, *Phys. Rev. D* 72 (2005) 015004 [arXiv:hep-ph/0504036]; A. Falkowski, O. Lebedev and Y. Mambrini, *JHEP* 0511 (2005) 034 [arXiv:hep-ph/0507110]; R. Kitano and Y. Nomura, *Phys. Lett. B* 631 (2005) 58 [arXiv:hep-ph/0509039]; R. Kitano and Y. Nomura, *Phys. Rev. D* 73 (2006) 095004 [arXiv:hep-ph/0602096]; A. Pierce and J. Thaler, *JHEP* 0609 (2006) 017 [arXiv:hep-ph/0604192]; K. Kawagoe and M. M. Nojiri, *Phys. Rev. D* 74, 115011 (2006)

- [arXiv:hep-ph/0606104]; H. Baer, E.-K. Park, X. Tata and T. T. Wang, JHEP 0608 (2006) 041 [arXiv:hep-ph/0604253]; K. Choi, K. Y. Lee, Y. Shimizu, Y. G. Kim and K. i. Okumura, JCAP 0612 (2006) 017 [arXiv:hep-ph/0609132]; O. Lebedev, V. Lowen, Y. Mambrini, H. P. Nilles and M. Ratz, JHEP 0702 (2007) 063 [arXiv:hep-ph/0612035].
- [5] M. Cvetič, A. Font, L. E. Ibanez, D. Lust and F. Quevedo, Nucl. Phys. B 361 (1991) 194; L. E. Ibanez and D. Lust, Nucl. Phys. B 382 (1992) 305 [arXiv:hep-th/9202046]; V. S. Kaplunovsky and J. Louis, Phys. Lett. B 306 (1993) 269 [arXiv:hep-th/9303040]; A. Brignole, L. E. Ibanez and C. Muñoz, Nucl. Phys. B 422 (1994) 125 [Erratum *ibid.* B 436 (1995) 747] [arXiv:hep-ph/9308271].
- [6] S. Dimopoulos and H. Georgi, Nucl. Phys. B 193, 150 (1981).
- [7] J. R. Ellis, K. A. Olive, Y. Santoso and V. C. Spanos, Phys. Lett. B 573 (2003) 162 [arXiv:hep-ph/0305212]; J. R. Ellis, K. A. Olive, Y. Santoso and V. C. Spanos, Phys. Rev. D 70 (2004) 055005 [arXiv:hep-ph/0405110].
- [8] E. Cremmer, S. Ferrara, C. Kounnas and D. V. Nanopoulos, Phys. Lett. B 133 (1983) 61; J. R. Ellis, A. B. Lahanas, D. V. Nanopoulos and K. Tamvakis, Phys. Lett. B 134 (1984) 429.
- [9] D. M. Ataliotakis and H. P. Nilles, Nucl. Phys. B 435 (1995) 115 [arXiv:hep-ph/9407251]; M. Olechowski and S. Pokorski, Phys. Lett. B 344, 201 (1995) [arXiv:hep-ph/9407404]; V. Berezinsky, A. Bottino, J. Ellis, N. Fornengo, G. Mignola and S. Scopel, Astropart. Phys. 5 (1996) 1, hep-ph/9508249; M. Drees, M. Nojiri, D. Roy and Y. Yamada, Phys. Rev. D 56 (1997) 276, [Erratum *ibid.* D 64 (1997) 039901], hep-ph/9701219; M. Drees, Y. Kin, M. Nojiri, D. Toya, K. Hasuko and T. Kobayashi, Phys. Rev. D 63 (2001) 035008, hep-ph/0007202; P. Nath and R. Amowitt, Phys. Rev. D 56 (1997) 2820, hep-ph/9701301; J. R. Ellis, T. Falk, G. Ganis, K. A. Olive and M. Schmitt, Phys. Rev. D 58 (1998) 095002 [arXiv:hep-ph/9801445]; J. R. Ellis, T. Falk, G. Ganis and K. A. Olive, Phys. Rev. D 62 (2000) 075010 [arXiv:hep-ph/0004169]; A. Bottino, F. Donato, N. Fornengo and S. Scopel, Phys. Rev. D 63 (2001) 125003, hep-ph/0010203; S. Profumo, Phys. Rev. D 68 (2003) 015006, hep-ph/0304071; D. Cerdeno and C. Muñoz, JHEP 0410 (2004) 015, hep-ph/0405057;
- [10] J. Ellis, K. Olive and Y. Santoso, Phys. Lett. B 539, 107 (2002) [arXiv:hep-ph/0204192]; J. R. Ellis, T. Falk, K. A. Olive and Y. Santoso, Nucl. Phys. B 652, 259 (2003) [arXiv:hep-ph/0210205].
- [11] H. Baer, A. Mustafayev, S. Profumo, A. Belyaev and X. Tata, Phys. Rev. D 71, 095008 (2005) [arXiv:hep-ph/0412059]. H. Baer, A. Mustafayev, S. Profumo, A. Belyaev and X. Tata, JHEP 0507 (2005) 065, hep-ph/0504001.
- [12] E. A. Baltz and P. Gondolo, JHEP 0410, 052 (2004) [arXiv:hep-ph/0407039]; B. C. Allanach, Phys. Lett. B 635, 123 (2006) [arXiv:hep-ph/0601089]; R. R. de Austri,

- R. Trotta and L. Roszkowski, *JHEP* 0605, 002 (2006) [arXiv:hep-ph/0602028]; B. C. Allanach, K. Cranmer, C. G. Lester and A. M. Weber, *JHEP* 0708, 023 (2007) [arXiv:0705.0487 [hep-ph]].
- [13] J. R. Ellis, K. A. Olive, Y. Santoso and V. C. Spanos, *Phys. Lett. B* 565 (2003) 176 [arXiv:hep-ph/0303043].
- [14] H. Baer and C. Balazs, arXiv:hep-ph/0303114; A. B. Lahanas and D. V. Nanopoulos, arXiv:hep-ph/0303130; U. Chattopadhyay, A. Corsetti and P. Nath, arXiv:hep-ph/0303201; C. Muñoz, hep-ph/0309346.
- [15] J. Dunkley et al. [WMAP Collaboration], arXiv:0803.0586 [astro-ph].
- [16] J. Ellis, T. Falk, and K. A. Olive, *Phys. Lett. B* 444 (1998) 367 [arXiv:hep-ph/9810360]; J. Ellis, T. Falk, K. A. Olive, and M. Srednicki, *Astr. Part. Phys.* 13 (2000) 181 [Erratum -ibid. 15 (2001) 413] [arXiv:hep-ph/9905481].
- [17] J. L. Feng, K. T. Matchev and T. Moroi, *Phys. Rev. D* 61 (2000) 075005 [arXiv:hep-ph/9909334].
- [18] V. D. Barger, M. S. Berger and P. Ohmann, *Phys. Rev. D* 49 (1994) 4908 [arXiv:hep-ph/9311269].
- [19] W. de Boer, R. Ehret and D. I. Kazakov, *Z. Phys. C* 67 (1995) 647 [arXiv:hep-ph/9405342].
- [20] M. Carena, J. R. Ellis, A. Pilaftsis and C. E. Wagner, *Nucl. Phys. B* 625 (2002) 345 [arXiv:hep-ph/0111245].
- [21] L. E. Ibanez, C. Lopez and C. Muñoz, *Nucl. Phys. B* 256 (1985) 218.
- [22] S. P. Martin and M. T. Vaughn, *Phys. Rev. D* 50 (1994) 2282 [arXiv:hep-ph/9311340].
- [23] Joint LEP 2 Supersymmetry Working Group, Combined LEP Chargino Results, up to 208 GeV, http://lepsusy.web.cern.ch/lepsusy/www/inos_moriond01/charginos_pub.html; LEP Higgs Working Group for Higgs boson searches, OPAL Collaboration, ALEPH Collaboration, DELPHI Collaboration and L3 Collaboration, *Phys. Lett. B* 565 (2003) 61 [arXiv:hep-ex/0306033]. Search for neutral Higgs bosons at LEP, paper submitted to ICHEP04, Beijing, LHWG-NOTE-2004-01, ALEPH-2004-008, DELPHI-2004-042, L3-NOTE-2820, OPAL-TN-744, http://lephiggs.web.cern.ch/LEPHIGGS/papers/August2004_MSSM/index.html.
- [24] G. Bennett et al. [The Muon $g-2$ Collaboration], *Phys. Rev. Lett.* 92 (2004) 161802, hep-ex/0401008; G. Bennett et al. [The Muon $g-2$ Collaboration], *Phys. Rev. D* 73 (2006) 072003 [arXiv:hep-ex/0602035].

- [25] S. Chen et al. [CLEO Collaboration], Phys. Rev. Lett. 87 (2001) 251807 [arXiv:hep-ex/0108032]; P. Koppenburg et al. [Belle Collaboration], Phys. Rev. Lett. 93 (2004) 061803 [arXiv:hep-ex/0403004]. B. Aubert et al. [BaBar Collaboration], arXiv:hep-ex/0207076; E. Barberio et al. [Heavy Flavor Averaging Group (HFAG)], arXiv:hep-ex/0603003.
- [26] ATLAS Collaboration, Detector and Physics Performance Technical Design Report, CERN/LHCC/99-15 (1999), see: <http://atlasinfo.cern.ch/Atlas/GROUPS/PHYSICS/TDR/access.html> ; M. Schumacher, Czech. J. Phys. 54 (2004) A103; arXiv:hep-ph/0410112; S. Abdullin et al., Eur. Phys. J. C 39S2 (2005) 41.
- [27] The CMS Collaboration, CMS Physics Technical Design Report. Volume II: Physics Performance, CERN/LHCC 2006-021, CMS TDR 8.2 (2006), see: <http://cmsdoc.cern.ch/cms/cpt/tdr/> .
- [28] J.-J. Blaising, A. De Roeck, J. Ellis, F. Gianotti, P. Janot, G. Rolandi, and D. Schlatter, Potential LHC Contributions to Europe's Future Strategy at the High Energy Frontier; J. Ellis, Physics at LHC , arXiv:hep-ph/0611237.
- [29] J. Aguilar-Saavedra et al., TESLA TDR Part 3: Physics at an e^+e^- Linear Collider, arXiv:hep-ph/0106315, see: <http://tesla.desy.de/tdr/> ; T. Abe et al. [American Linear Collider Working Group Collaboration], Resource book for Snowmass 2001, arXiv:hep-ex/0106055; K. Abe et al. [ACFA Linear Collider Working Group Collaboration], arXiv:hep-ph/0109166. S. Heinemyer et al., arXiv:hep-ph/0511332.
- [30] H. Goldberg, Phys. Rev. Lett. 50 (1983) 1419; J. Ellis, J. Hagelin, D. Nanopoulos, K. Olive and M. Srednicki, Nucl. Phys. B 238 (1984) 453.
- [31] H. Nilles, Phys. Rept. 110 (1984) 1; H. Haber and G. Kane, Phys. Rept. 117 (1985) 75; R. Barbieri, Riv. Nuovo Cim. 11 (1988) 1.
- [32] H. Baer, C. Balazs, A. Belyaev, T. Krupovnickas and X. Tata, JHEP 0306 (2003) 054 [arXiv:hep-ph/0304303].
- [33] D. M. Pierce, J. A. Bagger, K. T. Matchev and R. J. Zhang, Nucl. Phys. B 491, 3 (1997) [arXiv:hep-ph/9606211].
- [34] D. Tovey, Inclusive SUSY searches and measurements at ATLAS, Eur. Phys. J. direct C 4 CN4 (2002).
- [35] D. Tovey, private communication.
- [36] J. Brau et al., International Linear Collider reference design report. 1: Executive summary. 2: Physics at the ILC. 3: Accelerator. 4: Detectors, SLAC-R-857 (2007).